

FABRICATION OF SUPERHYDROPHOBIC GOLD FILM ON POLYMER SUBSTRATES



A Thesis Submitted in Partial Fulfillment of the Requirements
for the Degree of Master of Science in Petrochemistry and Polymer Science
Field of Study of Petrochemistry and Polymer Science
Faculty of Science
Chulalongkorn University
Academic Year 2018
Copyright of Chulalongkorn University

การสร้างฟิล์มทองคำไม่ชอบน้ำอย่างยั้งยวดบนพอลิเมอร์ซับสเตรต



วิทยานิพนธ์นี้เป็นส่วนหนึ่งของการศึกษาตามหลักสูตรปริญญาวิทยาศาสตรมหาบัณฑิต
สาขาวิชาปิโตรเคมีและวิทยาศาสตร์พอลิเมอร์ สาขาวิชาปิโตรเคมีและวิทยาศาสตร์พอลิเมอร์

คณะวิทยาศาสตร์ จุฬาลงกรณ์มหาวิทยาลัย

ปีการศึกษา 2561

ลิขสิทธิ์ของจุฬาลงกรณ์มหาวิทยาลัย

Thesis Title FABRICATION OF SUPERHYDROPHOBIC GOLD FILM ON
POLYMER SUBSTRATES
By Miss Siriwan Boonmeewiriyā
Field of Study Petrochemistry and Polymer Science
Thesis Advisor Associate Professor KANET WONGRAVEE, Ph.D.

Accepted by the Faculty of Science, Chulalongkorn University in Partial
Fulfillment of the Requirement for the Master of Science

..... Dean of the Faculty of Science
(Professor POLKIT SANGVANICH, Ph.D.)

THESIS COMMITTEE

..... Chairman
(Professor PATTARAPAN PRASASSARAKICH, Ph.D.)

..... Thesis Advisor
(Associate Professor KANET WONGRAVEE, Ph.D.)

..... Examiner
(Associate Professor NAPIDA HINCHIRANAN, Ph.D.)

..... External Examiner
(Suwussa Bamrungsap, Ph.D.)

ศิริวรรณ บุญมีวิริยะ : การสร้างฟิล์มทองคำไม่ชอบน้ำอย่างยิ่งยวดบนพอลิเมอร์ซับสเตรต. (FABRICATION OF SUPERHYDROPHOBIC GOLD FILM ON POLYMER SUBSTRATES) อ.ที่ปรึกษาหลัก : รศ. ดร.คณิศ วังษ์ระวี

งานวิจัยนี้ได้ศึกษาวิจัยและนำเสนอวิธีการสร้างพื้นผิวทองคำที่มีคุณสมบัติไม่ชอบน้ำอย่างยิ่งยวดบนพอลิไดเมทิลซิลิโคโนเซน โดยอาศัยปฏิกิริยารีดักชันระหว่างสารละลายกรดคลอโรอริก และสารละลายไซเตียมฟอร์เมตในการสังเคราะห์อนุภาคทองคำระดับไมโครเมตร โดยมีปัจจัยที่ต้องควบคุมในการเกิดปฏิกิริยาเพื่อให้ได้พื้นผิวทองคำที่มีคุณสมบัติไม่ชอบน้ำอย่างยิ่งยวด คือ สัดส่วนโดยโมลของสารตั้งต้นและระยะเวลาการทับถมกันของอนุภาคทองคำบนพื้นผิวพอลิไดเมทิลซิลิโคโนเซน หลังจากกระบวนการสร้างฟิล์มทองคำ แผ่นฟิล์มจะถูกตรวจสอบความชอบน้ำของพื้นผิวด้วยการตรวจวัดมุมสัมผัสของหยดน้ำบนพื้นผิว (water contact angle, WCA) และความแตกต่างของมุมสัมผัสของหยดน้ำในระหว่างการฉีดหยดน้ำออก และการดึงหยดน้ำกลับ (contact angle hysteresis) พบว่าคุณสมบัติความไม่ชอบน้ำอย่างยิ่งยวดบนพื้นผิวจะเกิดหลังจากกระบวนการทับถมผ่านไปเป็นระยะเวลา 2 ชั่วโมง และให้มุมของหยดน้ำบนพื้นผิวมีค่ามากกว่า 160 องศา ซึ่งจากวิธีที่ใช้ในการสร้างพื้นผิวไม่ชอบน้ำสามารถสร้างพื้นผิวทองคำที่มีค่ามุมสัมผัสของหยดน้ำบนพื้นผิวได้สูงถึง 164 องศา และค่าความแตกต่างของมุมสัมผัสของหยดน้ำกับพื้นผิวในระหว่างการฉีดออกและการดึงหยดน้ำกลับ มีค่าเพียงแค่ 2 องศา นอกจากนี้พื้นผิวทองคำจะถูกตรวจสอบลักษณะของโครงสร้าง และศึกษาข้อมูลเกี่ยวกับกระบวนการทับถมกันของอนุภาคทองคำบนพื้นผิวพอลิไดเมทิลซิลิโคโนเซนด้วยกล้องจุลทรรศน์อิเล็กตรอนแบบส่องกราด, เทคนิคการเลี้ยวเบนของรังสีเอ็กซ์แบบผง และอินฟราเรดสเปกโทรสโกปี การเกิดสมบัติที่ไม่ชอบน้ำของแผ่นฟิล์มทองคำดังกล่าวเกิดจากกระบวนการทับถมกันของทองคำโดยชั้นแรกจะเป็นการทับถมกันของอนุภาคทองคำทรงกลมที่กระจายตัวอยู่ทั่วบริเวณพื้นผิวอย่างเท่า ๆ กัน และโครงสร้างของทองคำในชั้นที่สองจะเป็นอนุภาคทองคำที่เป็นโครงสร้างแบบลำดับชั้นที่จะทำให้พื้นผิวมีความขรุขระและส่งผลให้พื้นผิวมีสมบัติไม่ชอบน้ำอย่างยิ่งยวด ความเสถียรของโครงสร้างทองคำแบบลำดับชั้นถูกทดสอบ พบว่าพื้นผิวยังคง

สาขาวิชา

ปีการศึกษา 2561

ลายมือชื่อ อ.ที่ปรึกษาหลัก

5972117923 : MAJOR PETROCHEMISTRY AND POLYMER SCIENCE

KEYWORD: Superhydrophobic surface, gold, polydimethylsiloxane, deposition reaction

Siriwan Boonmeewiriya : FABRICATION OF SUPERHYDROPHOBIC GOLD FILM ON POLYMER SUBSTRATES. Advisor: Assoc. Prof. KANET WONGRAVEE, Ph.D.

Superhydrophobic surface was fabricated by a reduction reaction between chloroauric acid (HAuCl_4) and sodium formate (HCOONa) on polydimethylsiloxane (PDMS) substrate without any further surface modification. This generated gold films with superhydrophobic properties examined by water contact angle (WCA) and contact angle hysteresis measurement. Wettability of the fabricated gold film on PDMS substrate can be controlled by the deposition time which provides the $\text{WCA} > 160^\circ$ and it could be up to 164.41° with a contact angle hysteresis of 1.93° when the deposition time was prolonged at least 2 hours. To propose the deposition mechanism, the morphological structure and chemical characters of the gold films at different deposition time was deeply investigated using scanning electron microscope (SEM), Energy Dispersed X-ray spectrometer (EDS), X-ray diffractometer (XRD) and infrared spectrophotometer (IR). The gold films contain two different layers including uniformly spherical particles and the secondary structure. The secondary structure is the key factor to control roughness and hydrophobicity of the gold films. The stability of the gold films was inspected by using water-drop testing. The gold films can be tolerated for 7,200 drops without any loss of hydrophobic properties. The potential applications of using the gold films as magneto-wetting surface and a powerful SERS substrate were demonstrated.

Field of Study: Petrochemistry and
Polymer Science

Student's Signature

Academic Year: 2018

Advisor's Signature

ACKNOWLEDGEMENTS

I would like to give a warm thank-you with my sincerity to all the people who have given me help and kind supporting. This thesis couldn't be complete without them.

First, I would like to express my deepest appreciation to my advisor, Associate Professor Dr. Kanet Wongravee who has been the sustained source of enthusiasm during the whole time of my master program. I am also indebted to him for his guidance and suggestions throughout my research. Furthermore, he always gives the powerful encouragement and advises smart ideas.

I would like to express my gratitude to Assistant Professor Dr. Prompong Pienpinijtham and Professor Dr. Sanong Ekgasit for the useful theoretical background and the improvement of presentation skills.

I would like to sincerely appreciate the committees who devote their time for being my thesis committee and give me a useful suggestion.

I would also convey my heartfelt gratefulness to all my beloved friends: Sensor Research Unit (SRU) for warm-hearted and spiritual supporting during this research. In particular, Dr. Supeera Nootchanat, Dr. Attasith Parnsubsakul, Miss Piyada Disara, Miss Pimchanok Laowtaweerungruang and Mr. Bhobnibhit Chatmaneerungcharoen who suggests the alternative ways for the planning of my experiments, reviewing the thesis and always light me with their joke.

Finally, I deeply appreciate my family for the unconditional love to me. No words are enough to thank you for their encouragement which pushes me through success. It is my fortune to be their daughter.

Siriwan Boonmeewiriya

TABLE OF CONTENTS

	Page
.....	iv
ABSTRACT (THAI).....	iv
.....	v
ABSTRACT (ENGLISH).....	v
ACKNOWLEDGEMENTS.....	vi
TABLE OF CONTENTS.....	vii
LIST OF TABLES.....	ix
LIST OF FIGURES.....	x
ABBREVIATIONS.....	xv
CHAPTER 1 INTRODUCTION.....	1
1.1 Objectives.....	8
1.2 Scope of this research.....	8
CHAPTER 2 THEORETICAL BACKGROUND.....	9
2.1 Wetting and water contact angle.....	9
2.2 Superhydrophobic surface.....	12
2.3 In-house goniometer and imageJ program with dropsnake plug-in.....	14
2.4 Polydimethylsiloxane (PDMS) as a low surface energy material.....	18
CHAPTER 3 EXPERIMENTAL SECTION.....	20
3.1 Chemicals and Materials.....	20
3.2 Instruments.....	21
3.3 Preparation of PDMS substrate.....	21

3.4 Fabrication of gold film on PDMS	22
3.5 Magnetowetting applying on the surface.....	23
3.6 Detection SERS spectra of PET on fabricated gold film.....	24
3.7 Characterizations	25
CHAPTER 4 RESULTS AND DISCUSSION.....	27
4.1 Substrates for fabrication superhydrophobic gold film	27
4.2 Fabrication of gold film on PDMS	28
4.2 Wettability of the gold film	37
4.3 Deposition mechanism of gold particles on PDMS.....	43
4.4 Stability of non-wetting properties	49
CHAPTER 5 CONCLUSIONS.....	56
REFERENCES	57
VITA.....	65

LIST OF TABLES

	Page
Tabel 3. 1 Comparison of Water contact angle measurement between standard goniometer and in-house goniometer on bared PDMS and gold film on PDMS.....	26
Table 4. 1 Calculated average crystallite size of gold particles from of gold film at different deposition time by using Debye-Scherrer formula.....	37
Table 4. 2 WCA, calculated roughness factor from Wenzel's theory, pictures of 2 μ L DI water on 0.5x0.5 cm^2 gold film and SEM images of morphology on gold film surface at different deposition time.....	42
Table 4. 3 WCA-Left, WCA-Right, WCA average and difference between WCA-Left and WCA-Right of ferromagnetic droplet on non-wetting gold film in different position.....	53

LIST OF FIGURES

	Page
Figure 1. 1 SEM images of PS-PDMS surface cast from a micellar solution(A) and the needle-like poly(alkylpyrrole) film by electrochemical polymerization(B).....	3
Figure 1. 2 SEM images of nanopillars and nanopits on silicone by electron beam lithography.....	4
Figure 1. 3 SEM images of lotus-like superhydrophobic metal surface by the electrochemical reaction with sulfur gas.....	5
Figure 1. 4 Magnetowetting phenoma on different magnetic field (a,b), magnetic droplet on controllable surface (c) and ferrofluid droplet on surface (d,e).....	7
Figure 2. 1 Water droplet on solid surface, interaction between molecules inside the droplet and interaction between the molecules on the surface.....	9
Figure 2. 2 Contact angle (θ) and three vectors of surface energy between interphases:surface energy between liquid and vapor (γ_{lv}), surface energy between solid and liquid (γ_{sl}) and surface energy between solid and vapor (γ_{sv}) and types of wettability on surface at different contact angle.....	10
Figure 2. 3 Pictures of droplet in advancing CA (Left) and receding CA (right)	11
Figure 2. 4 Water droplet on the rough surface: liquid infiltrate into the roughness (Wenzel's model; Left) and liquid suspends on the roughness (Cassie-Baxter's model; Right)	13

Figure 2. 5 Schematic shows each instrument of in-house goniometer.....	15
Figure 2. 6 Chemical Structure of polydimethylsiloxane (PDMS)	18
Figure 2. 7 Organometallic crosslinking reaction of polydimethylsiloxane (PDMS)	19
Figure 3. 1 Schematic drawing of the preparation of PDMS substrate by mixing of silicone elastomer base and silicone elastomer curing agent with ratio 10:1 by weight.....	22
Figure 3. 2 Schematic drawing of the preparation gold growth solution by using chloroauric acid as metal ion source and sodium formate as reducing agent and procedure of fabrication gold film on PDMS.....	23
Figure 3. 3 Schematic showed applying magnetowetting on fabricated superhydrophobic surface.....	24
Figure 4. 1 Images of substrates, gold film with 200 μL of AUGS and: glass slide (A1, A2), acrylic(B1, B2) and PDMS(C1,C2), images of water droplet on bared substrates and gold films on substrates: glass slide (D1,D2), acrylic (E1,E2) and PDMS (F1,F2) and graph showed WCA on bared substrates and gold films on each substrate(G).....	28
Figure 4. 2 Time lapse of growth solution with laser radiation (A) from 0-2 h with interval of 20 minutes.....	30
Figure 4. 3 Pictures of gold film, droplet of DI water and WCA and SEM images from the reaction between $[\text{AuCl}_4]^-$ and HCOONa at different concentration of HCOONa : 0.2 M (A1, B1, C1-C2), 1 M (A2, B2, D1-D2) and 5 M (A3, B3, E1-E2) respectively.....	31

Figure 4. 4 Images of gold film on free surface PDMS in different volume of AuGS (A): 50, 100, 200, 300, 400 and 1,000 μL (left-right), graph shows the relative between volume of gold growth solution and radius or area of gold films (B), SEM images of deposited gold particles on PDMS (C), EDX mapping from gold film (D) and gold film in different patterns (E).....	32
Figure 4. 5 IR spectrum of bared PDMS and Au film at 15 min and 4 h deposition time and Au film at 4 h deposition time with removed some gold particles on the surface.....	34
Figure 4. 6 EDX pattern and percent atom of elements obtains from the fabricated gold film at 4 h deposition time.....	35
Figure 4. 7 XRD pattern of PDMS (A1) and fabricated gold film at different deposition time: 30 min (A2), 2 h (A3) and 4 h (A4).....	36
Figure 4. 8 Optical images, pictures of water droplet and SEM images of fabricated gold film on $0.5 \times 0.5 \text{ cm}^2$ PDMS at different deposition time (A) and graph shows relative between WCA or roughness factor calculated using Wenzel's equation and deposition time (B) from 15 min-24 h (WCA on virgin PDMS = 108°).....	38
Figure 4. 9 Raw UV-Vis spectrum of fabricated gold film at different deposition time from 15 min-24 h and normalized UV-Vis spectrum of gold film at different deposition time from 15 min-4 h.....	39

- Figure 4. 10 Pictures of water droplet on the gold film for measuring dynamic CA: advancing way (A1) and receding way (A2) and graph shows the WCA of advancing and receding angle during the measurement time (B).....43
- Figure 4. 11 SEM images show the structure of deposited gold particles (A1) on the PDMS: gold particles on the first layer (A2) and secondary structure (A3).....44
- Figure 4. 12 SEM images of gold film on 0.5x0.5 cm² PDMS and distribution graph of particle size at different deposition time: 30 min (A1,A2), 45 min (B1,B2), 1 h (C1,C2), 2 h (D1,D2), 4 h (E1,E2), 8 h (F1,F2) and 24 h (G1,G2).....45
- Figure 4. 13 Fabricated gold film in DI water and SEM images before sonication (A1,A2) and after sonication 15 min (B1,B2) and SEM images of sonicated secondary structure from gold film (C1-C3).....46
- Figure 4. 14 Picture of deposition reaction AuMPs on 0.5x0.5 cm² PDMS at the top and bottom of gold growth solution for 2 hours deposition time (A), SEM images and pictures of gold film from the reaction: top position (B1,B2) and bottom position (C1,C2).....48
- Figure 4. 15 Schematic shows method for fabrication the superhydrophobic gold film on PDMS by reduction reaction between chloroauric acid and sodium formate.....49

Figure 4. 16 Schematic of durability test of fabricated superhydrophobic gold film by dropping the water at a rate 1 drop/1 sec for 2 h (A) and graph shows WCA of gold film in durability test in every 15 min for 2 h (B).....	50
Figure 4. 17 Frame by frame of droplet jumping on non-wetting gold film.....	50
Figure 4. 18 Frame by frame pictures of ferromagnetic droplet moving on superhydrophobic gold film with controlling by magnetic bar: top view (A1-A5) and side view (B1-B5) with horizontal surface and side view with changing the angle of surface (C1-C5).....	51
Figure 4. 19 Pictures of ferromagnetic droplet movement to pick up powder on non-wetting gold film.....	52
Figure 4. 20 Frame by frame of ferromagnetic droplet moving on non-wetting gold film in different position.....	53
Figure 4. 21 SERS spectrum of PATP on PDMS and fabricated gold film at different deposition time: 30 min, 2 h and 4 h (A) and 2D-Raman Spectrum of PATP on PDMS (B1), fabricated gold film at 30 min (B2), 2 h (B3) and 4 h (B4).....	55

ABBREVIATIONS

HAuCl ₄	chloroauric acid
HCOONa	sodium formate
HCOO ⁻	formate ion
NaBH ₄	sodium borohydride
PDMS	polydimethylsiloxane
PMMA	poly(methylmethacrylate)
PS	polystyrene
PANI	polyaniline
DI water	deionized water
AuMP	gold microparticle
AuNP	gold nanoparticle
AuGS	gold growth solution
Au ³⁺	gold (III) ion
Au ⁺	gold (I) ion
Au ⁰	metallic gold
AgNP	silver nanoparticle
CO ₂	carbon dioxide
SEM	scanning electron microscopy
EDX	energy dispersive X-ray spectroscopy
CA	contact angle
WCA	water contact angle
SERS	surface enhance raman spectroscopy
LED	light-emitted diode
UV	ultraviolet

E^0	standard electrode potential
SD	standard deviation
mL	milliliter
μL	microliter
M	molar
cm	centimeter
mm	millimeter
μm	micrometer
nm	nanometer
s	second
min	minute
h	hour
kV	kilovolt
keV	kiloelectron volt
mW	milliwatt
$^\circ$	degree
θ	theta

CHAPTER 1

INTRODUCTION

Superhydrophobicity is the significant property of the surface which comes with high Water Contact Angle (WCA) with $\theta > 150^\circ$, low contact angle hysteresis and low sliding angle¹. This non-wetting surface belongs with water repellent, self-cleaning, anti-sticking and anti-contaminant. All beneficial properties are required for several applications in industrial and biological field such as self-cleaning satellite dishes, solar cell or outer architectural glass and waterproof surface for textiles and blood vessel replacement. To express the non-wetting surface, the structure should be a cooperation between roughness with special micro- or nano-structure². In nature, a basic and good example representing of superhydrophobic surface is Lotus leaf but for the scientifically ways to create the superhydrophobic property on surface are explained in two different ways involving one is to make roughness on low surface energy materials and another is to modify a rough surface with low surface energy materials³. Low surface materials usually are fluorocarbon, silicone, polystyrene, zinc oxide or titanium oxide etc. and there are many methods to obtain roughness on surface such as lithography, etching, layer-by-layer, sol-gel processing, electrospinning etc. Both ways to create the roughness could be generated to serve the superhydrophobic property on surface are as follows.

Formation of roughness surface on low surface energy material

This technique is a formation of a rough surface from low surface energy materials and the example which was created a rough surface with this method showed in Figure 1.1. The materials of interest with low surface energy are fluorocarbons, silicones, organic materials and inorganic materials.

Fluorocarbons have very low surface energy (22 mN/m). The major and interesting material of fluorocarbon which are applied for superhydrophobic field is poly(tetrafluoroethylene) or Teflon. It can be used directly for the superhydrophobic surface fabrication such as stretching film or treating surface with oxygen-plasmon⁴⁻⁶. Moreover, linking or blending fluorinated materials with other materials are investigated^{7, 8}.

Silicones or polydimethylsiloxane (PDMS) is a polymer with low surface energy. The superhydrophobic property from silicones occurred from treating or making the roughness on surface by laser etching or nanocasting method⁹⁻¹¹. On the other hand, silicones are used as the block polymers by blending with polystyrene (PS)^{12, 13}.

Paraffinic hydrocarbons which are organic materials are proposed and examined for superhydrophobic surface. Controlling the crystallization behavior of polyethylene (PE) by adding cyclohexanone to making floral-like crystal nanostructure can fabricate porous superhydrophobic surface with WCA 173¹⁴. The other way to utilize the organic materials for superhydrophobic surface are electrostatic spinning and spraying the polystyrene (PS) solution in dimethylformamide to obtain porous micro-/nano-fiber^{15, 16}. Moreover, polyamide, polycarbonate, alkylketene dimer or poly(alkylpyrrole) can be used into superhydrophobic surface¹⁷⁻²⁰.

Inorganic materials such as zinc oxide (ZnO) or titanium oxide (TiO₂) produced the superhydrophobic property. The ZnO nanorods in film can create roughness and 001 plane of nanorod is obviously the low surface energy^{21, 22}. Similar with TiO₂, the superhydrophobic surface can be achieved by making TiO₂ nanorod films²³.

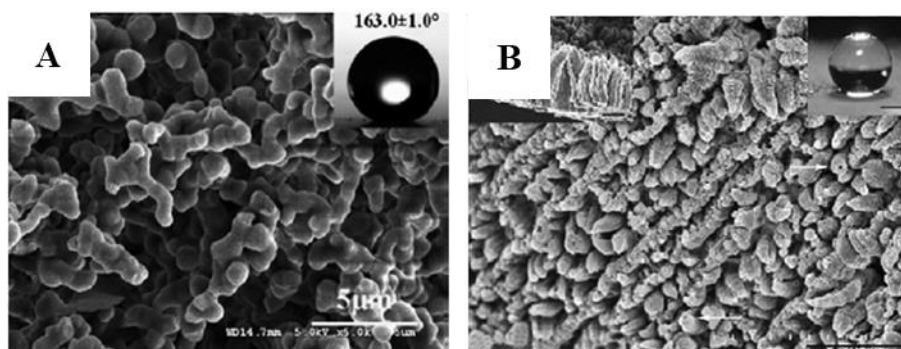


Figure 1.1 SEM images of PS-PDMS surface cast from a micellar solution(A)¹³ and the needle-like poly(alkylpyrrole) film by electrochemical polymerization(B)¹⁸

Formation of roughness and modifying surface on low surface energy material

The superhydrophobic surface can be fabricated by modifying a rough surface with low surface energy material. Normally, it can classify the fabrication of a rough surface into 2 categories: top-down and bottom-up approaches which can be fabricated by various strategies including Etching, Lithography, Sol-gel processing, Layer-by-layer, Colloidal assembly, Electrochemical reaction and deposition, Electrospinning and Chemical/physical vapor deposition.

Top-down approach

Top-down approach is referred to carve the materials with tools and lasers. Etching and lithography have been used for the formation of superhydrophobic surface. Etching is a simple and effective method to obtain the roughness on surface. There are different ways to form roughness by etching such as plasma etching²⁴, laser etching²⁵ or chemical etching^{26, 27}. The case of lithography such as photolithography, electron beam lithography, X-ray lithography, soft lithography, nanosphere lithography, etc is the technique to create micro-/nanopatterns on the large-area²⁸⁻³⁰. Figure 1.2 showed the example of fabricated rough surfaces from top-down approach.

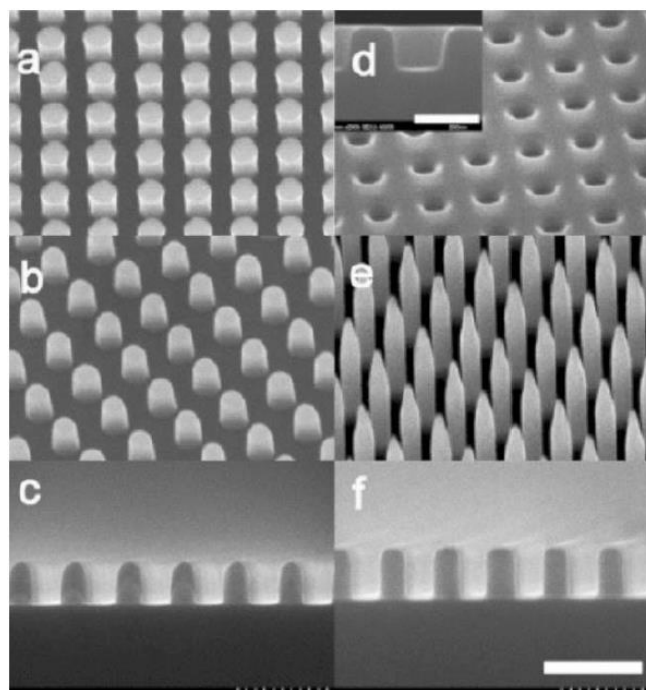


Figure 1. 2 SEM images of nanopillars and nanopits on silicone by electron beam lithography³⁰

Bottom-up approach

Bottom-up approach is described as the generation of stable and more complex structure by self-assembly of smaller building blocks. This approach has been used for the generation of superhydrophobic surface in several methods as shown in Figure 1.3 for example sol-gel processing, layer-by-layer deposition, colloidal assembly and chemical deposition. Sol-gel processing is the method for the gel forming by hydrolysis of the corresponding oxide in the large amount of solvent and impregnation of the solvent in the system. The illustrations to apply this method for superhydrophobic surface are to create porous sol-gel foam from organo-triethoxysilanes³¹ or to create the sol-gel film by using colloidal silica particles and fluoroalkylsilane³². For the layer-by-layer technique, it involves the electrostatic charge interactions between the layers. It can apply for superhydrophobic surface forming such as the generation of the honeycomb-like structure of poly(allylamine

hydrochloride)/poly(acrylic acid) (PAH/PAA) multilayer by acidic treatment³³. Chemical deposition is a chemical reaction and forming the product by self-assembly and deposition on the substrates. It has several methods for this technique such as chemical bath deposition, chemical vapor deposition or electrochemical deposition. The lotus-like superhydrophobic metal surface from the electrochemical reaction with sulfur gas and treatment of Cu/Cu-Sn alloy plated on steel sheets³⁴ is fabricated by this technique. Moreover, the roughness on surface can be forming by the combination of top-down and bottom-up approaches such as chemical vapor deposition method³⁵, micelles¹³ or electrospinning¹².

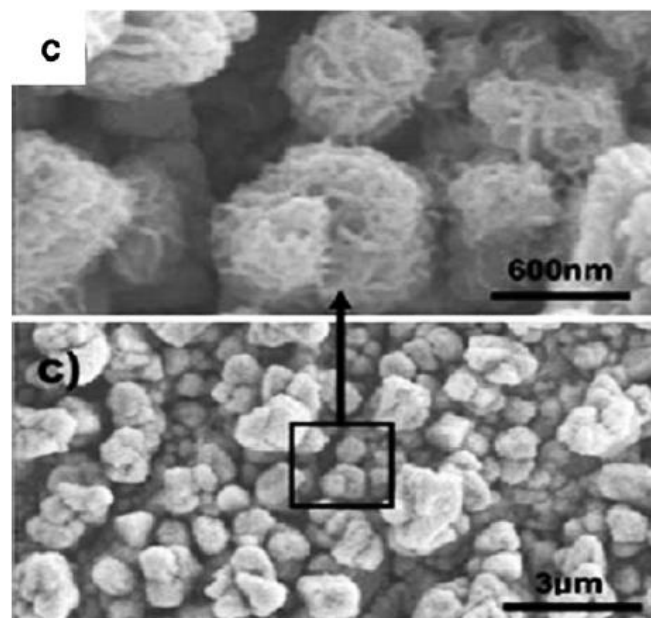


Figure 1. 3 SEM images of lotus-like superhydrophobic metal surface by the electrochemical reaction with sulfur gas³⁴

However, these methods are complicated and involve high-cost instruments to generate the roughness pattern on the surface. Consequently, another method to fabricate to superhydrophobic surface in a more simple, easier and lower cost is deposition. This approach can be used in several types of substrate that they can be either solid, metal or polymer substrates. Especially, deposition of micro- or nano-

particles on substrates was studied widely and it was applied in many applications³⁶⁻³⁹ such as electronic, sensor, catalyst or surface enhance raman spectroscopy (SERS) substrate. Abdelsalam et al.⁴⁰ deposited the structure of gold on submicrometer sphere template by electrochemical deposition. Cui et al.⁴¹ constructed the superhydrophobic surface by using chemical deposition of gold nanoflower on iron foil and it obtained WCA up to 169^o. Moreover, all kind of materials were used as a substrate for deposited gold and polymer was the one of choices was studied about deposition gold on the surface. In 2008, Ishida, et al.⁴² deposited gold nanoparticles directly on several types of polymer bead and performed to use them as a catalyst. Deore, et al.⁴³ synthesized and coated gold nanoparticles on PVA sheet by using low energy electron radiation technique and recently, Ahmed et al.⁴⁴ immersed the substrates such as glass or silicones into gold solution to deposit the gold nanoparticles on those substrates and modified the surfaces to study about the changing of wettability.

According to these methods, they can provide superhydrophobic property on surface which water droplet should be roll off on this surface without any external supervisions. One application which needs droplet controlling in microchannel with homogeneous movement is called microfluidic, and it has been studied and improved method to drive the droplet in many ways, especially driving the droplet by using magnetism^{45, 46} (Figure 1.4) as this method requires only magnetic particles inside the solution and external magnetic field to drive the droplet without high pressure or any supervisions. Recently, there has been research about synthesized the gold nanoparticles composite on PDMS to use in microfluidic systems⁴⁷. The film has interesting properties which can be applied in optical devices, immunoassays and other bioassays on PDMS-based microchips.

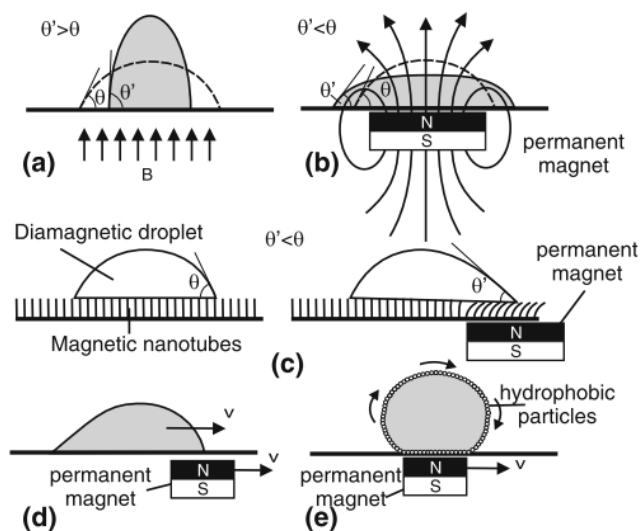


Figure 1. 4 Magnetowetting phenomena on different magnetic field (a,b), magnetic droplet on controllable surface (c) and ferrofluid droplet on surface (d,e)⁴⁵

This research is focused on modifying a rough gold film on low surface energy substrate which is PDMS. Superhydrophobic surface was fabricated with rapid and simple method by using chemical deposition of gold nanoparticles (AuNPs) on polydimethylsiloxane (PDMS). The AuNPs were synthesized by reduction reaction with only two chemicals were required in the process which were chloroauric acid (HAuCl_4) and sodium formate (HCOONa). The whole reaction was prepared at room temperature without special instruments. We studied about the homogeneity of the surface by changing shape of fabricated gold film with using different volumes of gold growth solution and pattern to create gold film. To obtain the superhydrophobic property, the ratio of reactants and deposition time of gold particles were investigated and optimized carefully. WCA and contact angle hysteresis were measured to examine the superhydrophobicity. Furthermore, the mechanism of gold particles deposition and the interaction between gold particles and PDMS were proposed. Some special applications like magnetowetting to control

wettability on surface and a SERS substrate to detect PET in water were demonstrated.

1.1 Objectives

1. To fabricate the superhydrophobic gold film on PDMS substrate using simple and rapid chemical reactions
2. To investigate the deposition mechanism of gold particles on PDMS surface in order to obtain the gold film with superhydrophobic property.
3. To control wettability on fabricated superhydrophobic gold film by using magnetowetting method.
4. To examine the efficiency of the superhydrophobic gold film as a SERS substrate.

1.2 Scope of this research

Superhydrophobic gold film was synthesized using chemical reduction between chloroauric acid and sodium formate on only PDMS substrate. The mole ratio of the reactants and reaction temperature are constrained. The superhydrophobicity of the generated gold film was inspected by static and dynamic water contact angle (WCA) measured by using in-house goniometer. Magnetowetting method was used to access the controlled wettability of the gold films. The efficiency of the gold film used as a powerful SERS substrate was examined for detection of *p*-aminothiophenol (PATP).

CHAPTER 2

THEORETICAL BACKGROUND

2.1 Wetting and water contact angle

Every surface has surface energy which is the contractile forces for pulling on the molecules of the surface. The surface energy is caused by the cohesive force between the molecules on the surface. Molecules inside droplet are balanced by neighboring molecules and have equal force in every direction so it has zero net force. However, molecules on the surface are not surrounded with neighboring molecules in every direction, so they have unbalanced force and form a higher energy on the surface. To minimize the energy on surface, the water adjusts its shape into the lowest surface energy and smallest surface area for a fixed volume with this incidence water droplet is formed a spherical shape on solid surface as shown in Figure 2.1, so it forms in spherical.

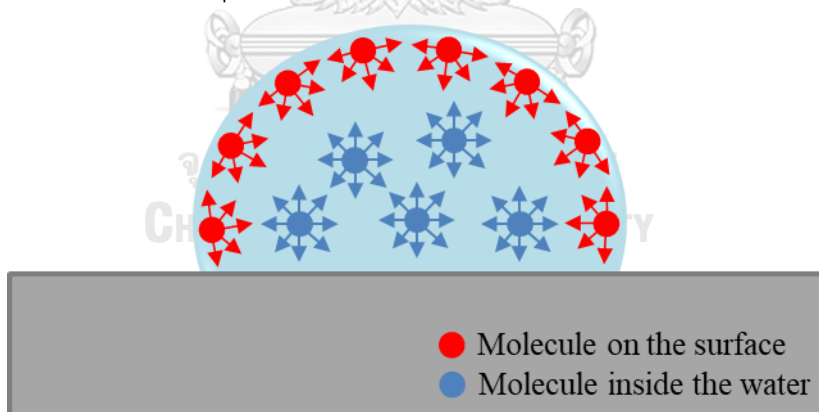


Figure 2. 1 Water droplet on solid surface, interaction between molecules inside the droplet and interaction between the molecules on the surface.

On the other hand, wetting is the ability to spread out of liquid on solid surface⁴⁸. It is related to surface energy and refer to balance of intermolecular forces which are adhesion force between solid surface and liquid and cohesion force between molecules of liquid. When the water contacts on the surface, it formed spherical cap and it deals with 3 phases of materials. Each of materials has interphase between two phases and create the surface energy which shows in Figure 2.2

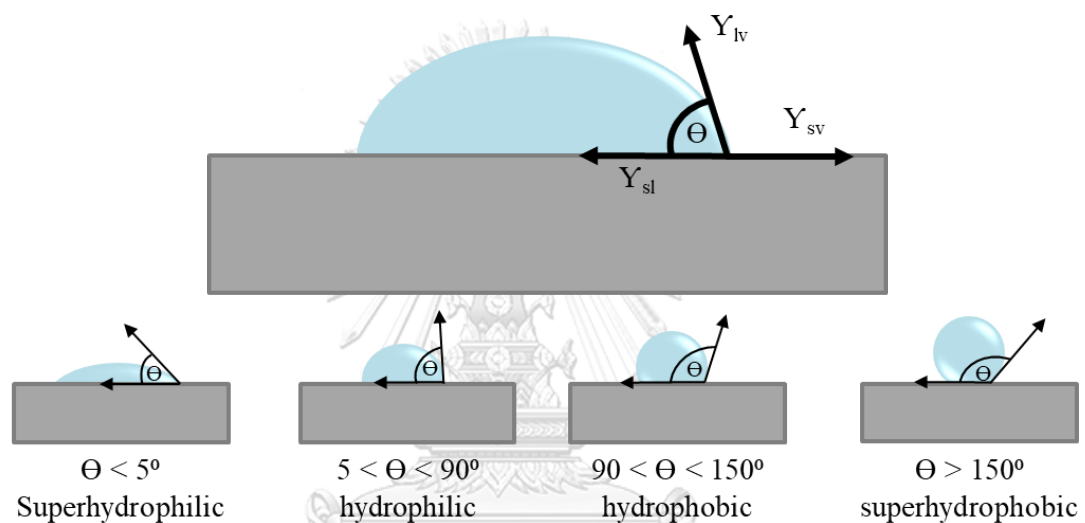


Figure 2. 2 Contact angle (θ) and three vectors of surface energy between interphases:surface energy between liquid and vapor (Y_{lv}), surface energy between solid and liquid (Y_{sl}) and surface energy between solid and vapor (Y_{sv}) and types of wettability on surface at different contact angle.

At the contact point, the interphase is referred to three-phase contact line. It has interfacial surface tensions among solid (s), liquid (l) and vapor (v) which are surface energy between liquid and vapor (Y_{lv}), surface energy between solid and liquid (Y_{sl}) and surface energy between solid and vapor (Y_{sv}). The angle between three phases is called contact angle (θ). Three vectors can balance the force in x direction (Eq.1) and rearrange to Young's equation⁴⁹ (Eq.2).

$$\Sigma F_x = Y_{sl} + Y_{lv} \cos \theta - Y_{sv} = 0 \quad \text{Eq.1}$$

$$Y_{lv} \cos \theta = Y_{sv} - Y_{sl} \quad \text{Eq.2}$$

The degree of wetting on surface can be defined by the value of water contact angle (WCA). The water pretends to spread out when the WCA is less than 90° . The water is rolled up and formed a spherical shape on the surface while the contact angle (CA) is larger than 90° . Based on CA, type of surface can classify into 4 main types: superhydrophilic ($\theta < 5^\circ$), hydrophilic ($5^\circ < \theta < 90^\circ$), hydrophobic ($90^\circ < \theta < 150^\circ$) and superhydrophobic ($\theta > 150^\circ$) as shown in Figure 2.2.

For ideal flat surface, static contact angles (static CAs) are equal to θ but the observed contact angle on real surface is not equal to θ because it is not just static state. Liquid on the fresh surface is in the actual motion and the contact angle at the three-phase contact line is called dynamic contact angle. The dynamic contact angle can be measured in various speed during inserting and pulling off the tip though the droplet which are called advancing contact angle (advancing CA, θ_a) and receding contact angle (receding CA, θ_r) as shown in Figure 2.3

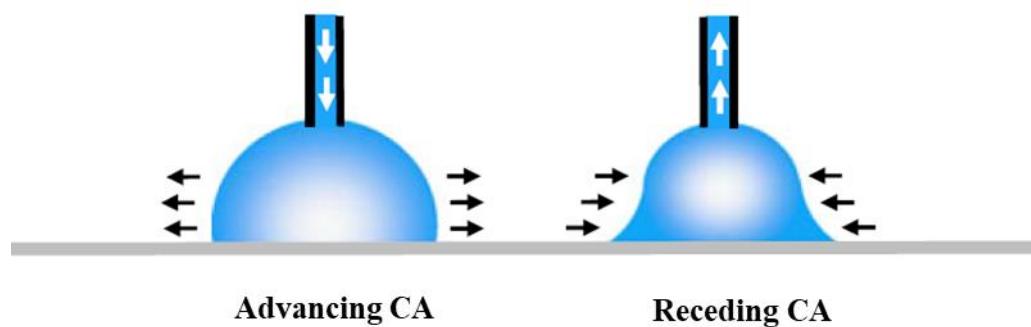


Figure 2. 3 Pictures of droplet in advancing CA (Left) and receding CA (right) ⁴⁸

If the dynamic CAs are measured in lower speed, the angle should be similar to static CAs. The different angle between θ_a and θ_r is called as the hysteresis (H) (Eq.3)

$$H = \theta_a - \theta_r \quad \text{Eq.3}$$

The surface with roughness or heterogeneity has the hysteresis^{50, 51}. For example, the droplet on hydrophobic surface is pinned at the contact point so the CA leads to increase at advancing motion and decrease at receding motion in the observed CA. However, it does not have the contact angle hysteresis on ideal flat surface and the observed CA is Young's angle.

For making the surface with superhydrophilic or superhydrophobic, it has 2 factors. First, it is surface chemistry that refers the surface has high or low surface energy. In general, surface with low surface energy will provide the superhydrophobicity. Second, it is surface roughness. The roughness on the surface can strongly initiate the hydrophobicity. The higher roughness, the larger hydrophobic of the surface occurs.

2.2 Superhydrophobic surface

The general way to determine the surface with superhydrophobic is WCA. Superhydrophobic surface is defined by WCA over 150° , a low sliding angle and a low contact angle hysteresis^{1, 52}. With a unique property of non-wetting surface such as self-cleaning effect, anti-sticking and anti-contamination. Superhydrophobic surface is of interesting in many applications including waterproofing textiles, blood vessel replacement, satellite dishes and exterior architectural glass. Generally, there are many hydrophobic surfaces in nature. Lotus leaf is a good example to express the superhydrophobicity on the surface as well as the wings of butterflies and the leaf of cabbage.

The surface with superhydrophobicity is typically rough in micro- or nano-scale. While presence of water droplet, the drop is remained on the surface which can be explained by two theories. The basic guideline for studying superhydrophobic surface would be explained in 2 theories which are Wenzel's theory⁵³ and Cassie-Baxter's theory⁵⁴ (Figure 2.4).

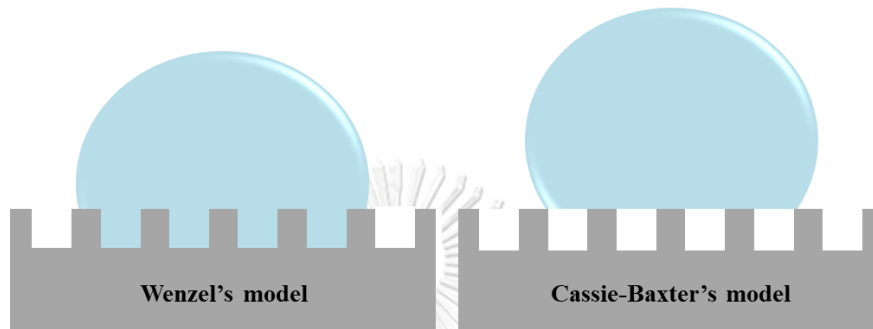


Figure 2. 4 Water droplet on the rough surface: liquid infiltrate into the roughness (Wenzel's model; Left) and liquid suspends on the roughness (Cassie-Baxter's model; Right)

In Wenzel's theory, the droplet can penetrate the roughness on surface. The water completely contacts with the surface and no air bubble between the surface and droplet. The calculation roughness in Wenzel's theory is defined by ratio between real surface area and projected surface area. In the real surface, every surface has some roughness (no surface is completely smooth) so the roughness is always more than 1. The Wenzel's equation shows the linear relation between roughness and apparent contact angle in Eq.4

$$r = \frac{\text{Real surface energy}}{\text{Projected surface energy}} \quad \text{Eq.4}$$

$$\cos \theta^* = r \cos \theta \quad \text{Eq.5}$$

In Wenzel's equation, the θ^* , θ and r are referred to apparent contact angle, equilibrium contact angle and roughness, respectively.

When the roughness is greater than 1, the value of $\cos \theta^*$ should be more than $\cos \theta$. In case of hydrophilic surface, $\theta^* < \theta < 90^\circ$, while value of $\theta^* > \theta > 90^\circ$ for case of hydrophobic surface. From Wenzel's state², the roughness on surface will always enhance the CA. When the roughness is more than 1.7, the surface tends to change from Wenzel's model into Cassie-Baxter's model. The surface possesses more roughness and possibility to promote more air-fraction on the droplet of water. At this stage, the drop can easily roll off on surface so that is useful for having water-repellent and self-cleaning effect on surface.

In Cassie-Baxter's model, θ^* depends on percent of solid that contacts with the droplet (Eq.5). f is defined as solid fraction.

$$\cos \theta^* = f(1 + \cos \theta) - 1 \quad \text{Eq.6}$$

When the droplet touches on the surface as small as possible or the droplet almost suspends on the air pocket, the $\cos \theta^*$ reaches to -1 indicating that the θ^* reaches to 180° and f reaches to zero. It refers the surface is completely non-wetting.

2.3 In-house goniometer and imageJ program with dropsnake plug-in

For water contact angle measurement in this research, in-house goniometer was built with 4 instruments in the same order as shown in Figure 2.5. LED light source with diffuser filter was placed at the backside of droplet in order to gain the highest contrast between droplet and background. Second section was a stage for placing the sample which were always parallelized. Third was the water injector composing of syringe and standing for dropping the water on a substrate. The last part was Nikon D90 digital camera with macro lens used for capturing the pictures of droplet on the surface. All instruments were parallelized in the same plane and were controlled flat plane with leveler.

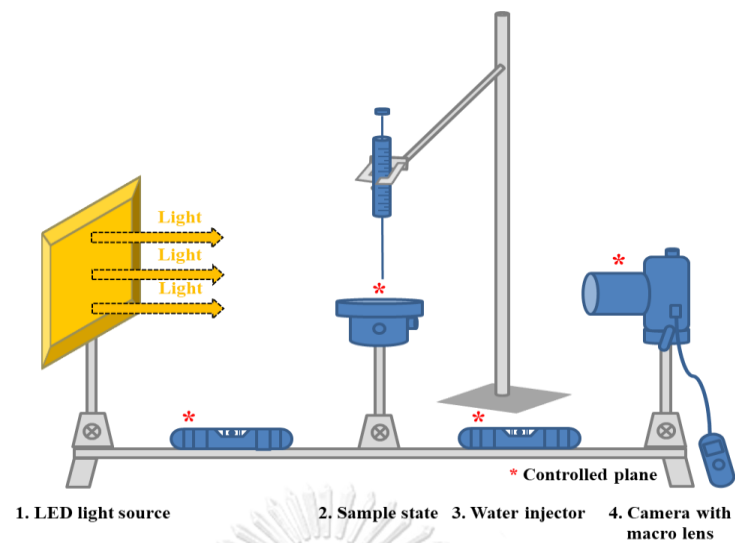
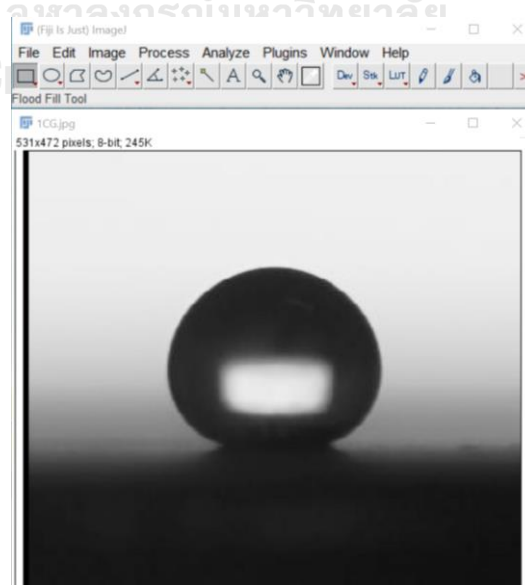


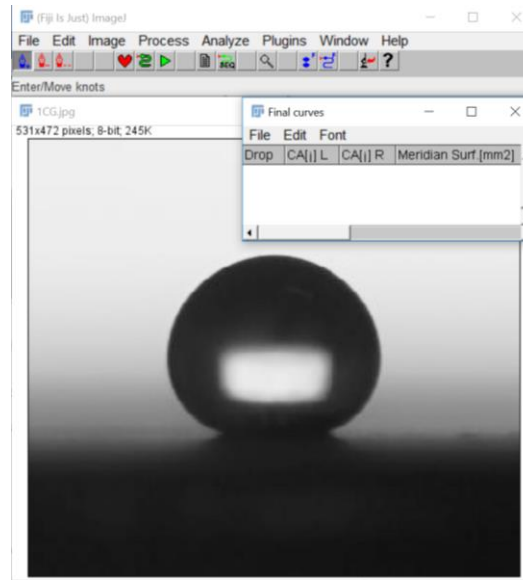
Figure 2. 5 Schematic shows each instrument of in-house goniometer

Photo of a droplet captured from the experiment were imported to the program for WCA measurement. The contrast of photo initially was enhanced by shift the color tone to black and white. Then, the WCA of a droplet were evaluated in imageJ program with dropsnake plug-in by following these steps.

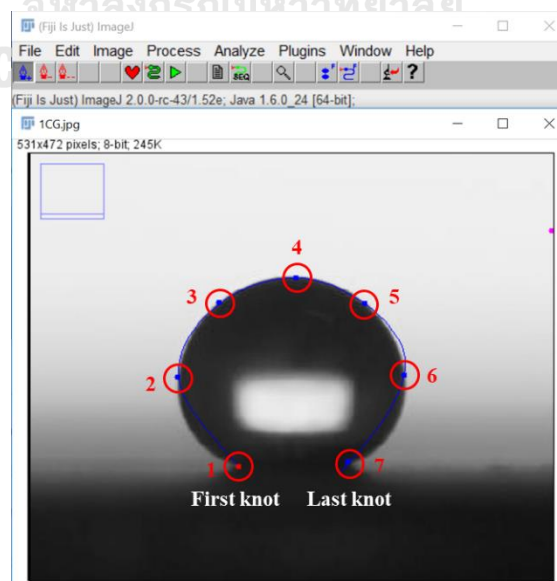
1. The imageJ program with dropsnake plug-in had to be set up and ready to use. Then, picture of droplet was imported to the program as shown.



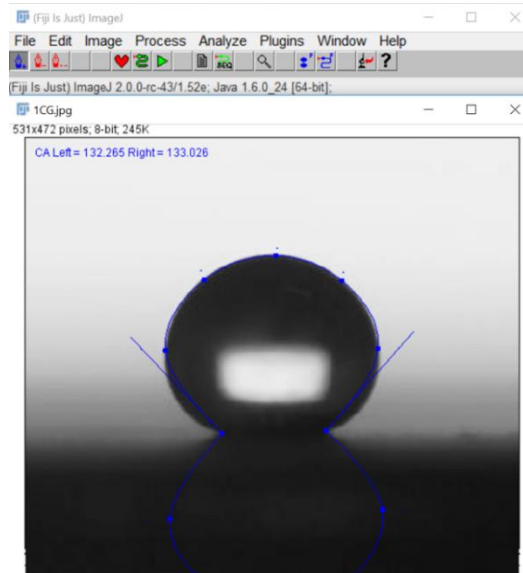
2. The dropsnake plugin was opened and then perform drop analysis and drop analysis-dropsnake, respectively. The new window which is called final curves will pop up. The information in new window will tell about the value of contact angle of droplet on the left handside ($CA_{(l)}$) and on the right handside ($CA_{(r)}$)



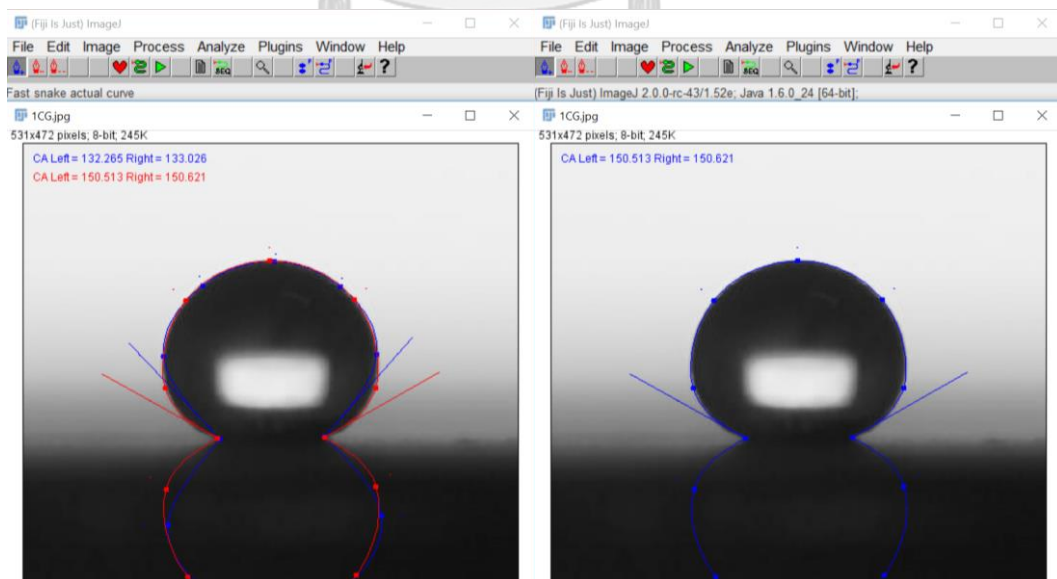
3. Create knots around the droplet. Number of knots on droplet should be 5-10 knots and the first and last knots should be pointed at the position which drop was touching on the surface. Optimized number of knots for this study was 7 knots.



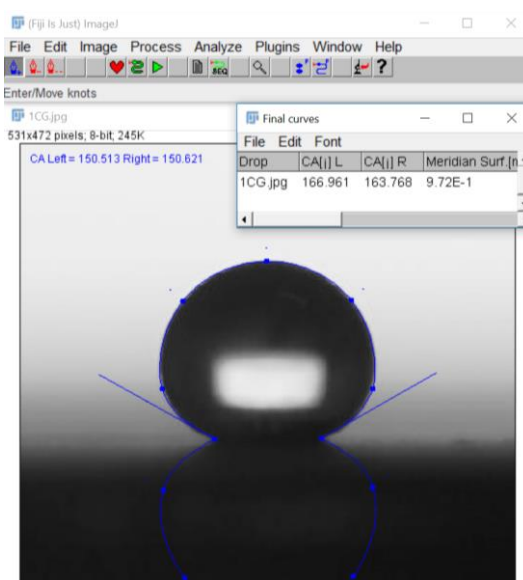
4. After knots were created around the droplet, clicking on the started knot should be done and the initial spline will be observed.



5. Run the fast snake actual curve on menu bar to improve the spline around curvature on the droplet. The initial spline should be fit with the droplet curvature and it showed the red line around the droplet. Otherwise, knots could be roughly adjusted. If it is satisfied, then click on accept red snake.



6. Press snake the curve to evolve the curve on droplet, then WCA value will be showed on the table and left- and right- contact angle ($CA_{(l)}$, $CA_{(r)}$) will be observed.



2.4 Polydimethylsiloxane (PDMS) as a low surface energy material

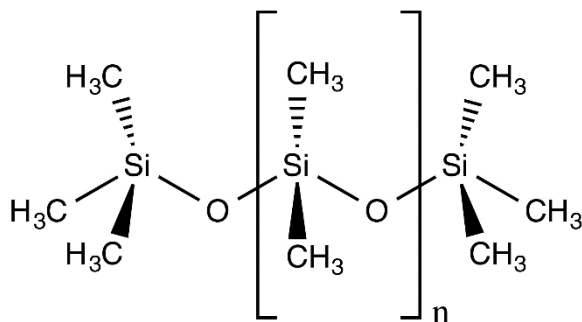


Figure 2. 6 Chemical Structure of polydimethylsiloxane (PDMS)

IUPAC name: Polydimethylsiloxane (PDMS)

Chemical formula: $(C_2H_6OSi)_n$

Density: 965 kg/m^3

PDMS⁵⁵ or silicones is the polymeric organosilicon compound which is a liquid with clear, viscosity, inert, non-toxic and non-flammable. It's applied in several applications such as contact lenses, medical device, heat-resistant tiles, caulking, antifoaming agent in food or material for making hair shiny and slippery in shampoos. It can be formed in solid from cross-linked polymer chain by an organometallic crosslinking reaction with trimethylsilyl chloride (showed in Eq.7)

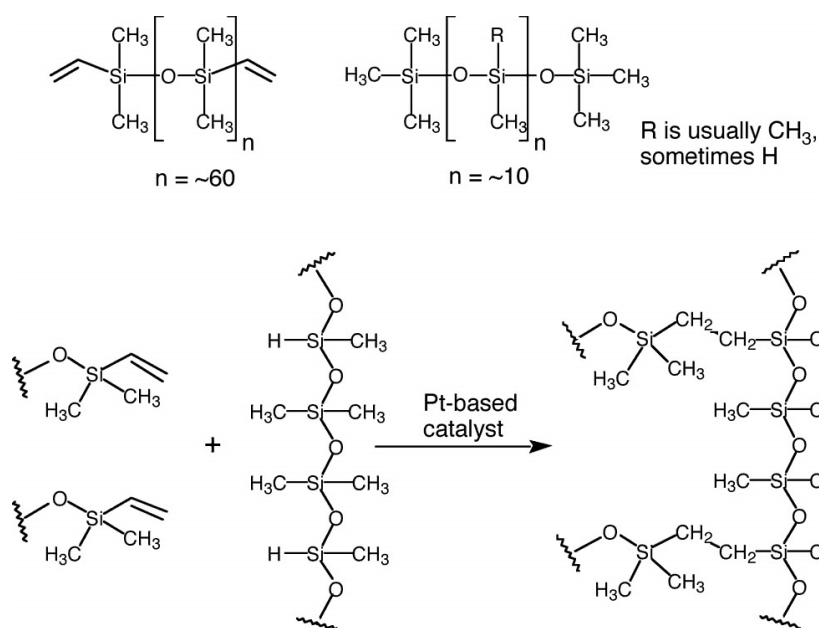


Figure 2. 7 Organometallic crosslinking reaction of polydimethylsiloxane (PDMS)

CHULALONGKORN UNIVERSITY

The solid PDMS after curing is obviously clear and flexible. The backbone structure of PDMS is formed the cross-linked structure with siloxane linkage. It achieves the flexible molecular structure and it's more flexible when molecular is higher. The surface of solid PDMS presents the hydrophobic property. The aqueous solvent can't spread out easily on the PDMS surface unless the organic solvent because it swells with organic solvent^{56, 57}.

CHAPTER 3

EXPERIMENTAL SECTION

3.1 Chemicals and Materials

1. Gold (III) chloride trihydrate ($\text{HAuCl}_4 \cdot 3\text{H}_2\text{O}$, $\geq 99.9\%$) (Sigma-Aldrich Co. LLC.)
2. Sodium formate (HCOONa) (Sigma-Aldrich Co. LLC.)
3. Polydimethylsiloxane (PDMS) (DOW Corning corporation)
4. Iron oxide nanoparticles
5. p-Aminothiophenol (PATP)
6. Silver nanoparticles (AgNPs)

Gold (III) chloride trihydrate, sodium formate and polydimethylsiloxane were analytical grade and used without further purification. Iron oxide nanoparticles were obtained from Bawendi's group⁵⁸ and PET was obtained from recycle plastic glass. Glassware and magnetic bars were always cleaned with liquid detergent and then rinsed with deionized (DI) water before using.

Silver nanoparticles (AgNPs)⁵⁹ was synthesized by starting the preparation of silver seed. Ultrapure water, silver nitrate (AgNO_3) and sodium citrate ($\text{C}_{18}\text{H}_{15}\text{Na}_9\text{O}_{21}$) were mixed in the flask and stirred in the ice bath for 30 min. Then, drop-wise of freshly prepared sodium borohydride with ice-cold ultrapure water was added into the mixture over 4 min. Ag solution was stirred on the ice bath for 2 min and color of solution turned from colorless into bright yellow. Therefore, the spherical silver nanoparticles colloids were obtained.

3.2 Instruments

1. Scanning Electron Microscope (SEM), JEOL JSM-6510A
2. Built-in energy dispersive X-ray spectrometer (EDX), JEOL JSM-6510A
3. High performance optical microscope (OM), Axio Scope.A1
4. In-house goniometer
5. Portable fiber optics spectrometer, Oean Optics USB400
6. X-ray diffractometer (XRD), Rigaku Model: D/Max-2200
7. Infrared spectrophotometer, Thermo scientific Nicolet iS5
8. Raman microscope, Thermo scientific DXR with 532 nm as excitation laser
9. Ultrasonic bath, Elmasonic Model: P30H
10. Vacuum Chamber

3.3 Preparation of PDMS substrate

To prepare a PDMS substrate, Sylgard 184 silicone elastomer base and curing agent were mixed in ratio 10:1 by weight⁶⁰⁻⁶². Silicone base was poured in plastic container and then curing agent was immediately added. The liquid was mixed by cleaned stirring rod until the large amount of bubbles were appeared (around 5 minutes). The mixture of PDMS liquid was poured into 8.5 cm diameter petri-dish plastic and then was degassed in vacuum chamber until all of gas bubbles disappeared. The curing process of PDMS elastomers was incubated under room temperature for 12 hours. The stable and transparent PDMS film with 1 mm thickness without liquid component was achieved and then was ready to be cut in a desired shape. The scheme of PDMS preparation is illustrated in Figure 3.1.

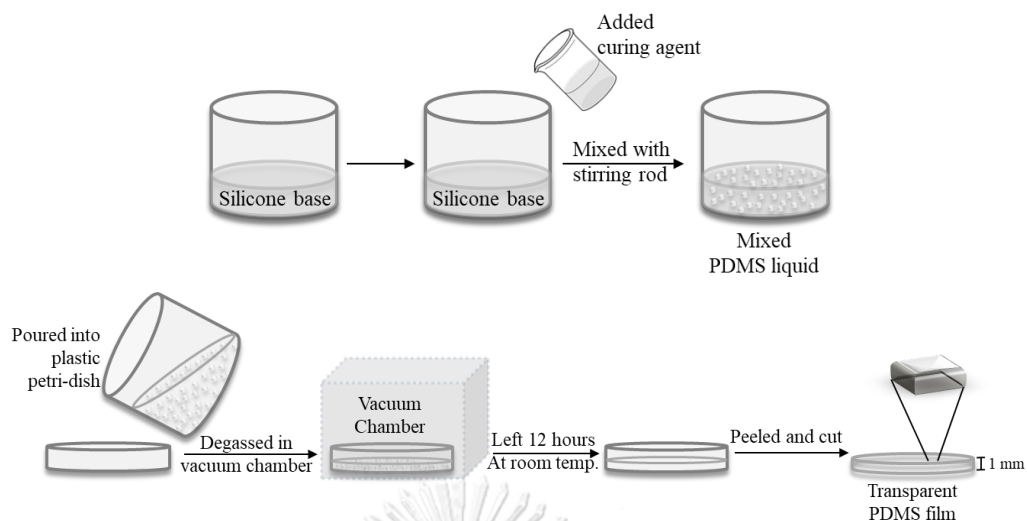


Figure 3. 1 Schematic drawing of the preparation of PDMS substrate by mixing of silicone elastomer base and silicone elastomer curing agent with ratio 10:1 by weight.

3.4 Fabrication of gold film on PDMS

Gold film on PDMS was fabricated by a simple wet chemical method using HCOONa as a reducing agent and stabilizing agent with HAuCl_4 as gold ion sources. The gold growth solution (AuGS) was freshly prepared by mixing HAuCl_4 (9.75 mL, 1M) and HCOONa (0.24 mL, 0.5M). The mole ratio of gold ions and formate was kept at 1:80 and pH of AuGS was about 5.19. The procedure of fabrication gold film started with drop of gold growth solution on PDMS with desired volume. The reduction and deposition reactions continued 4 h with prevention the evaporation by adding some water around PDMS substrate during the reaction, then the film was cleaned of excess solution by DI water and dried in vacuum chamber as shown in Figure 3.2. The deposited gold film was studied. The relative between dropped volume of AuGS and film area, deposition time, deposition mechanism of gold particles on PDMS and structure evolution of gold film at different time deposition.

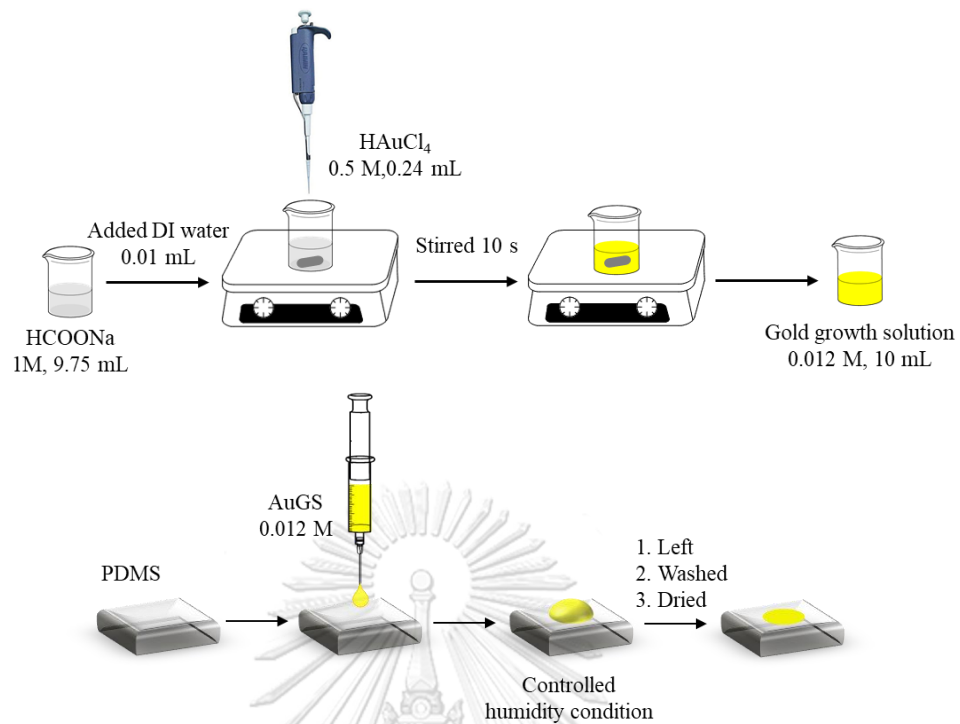


Figure 3. 2 Schematic drawing of the preparation gold growth solution by using chloroauric acid as metal ion source and sodium formate as reducing agent and procedure of fabrication gold film on PDMS.

3.5 Magnetowetting applying on the surface

Magnetowetting method was applied with non-wetting gold film (Figure 3.3) by using ferrofluid was received from iron oxide nanoparticles colloid. 10 μL droplet of ferrofluid was handled the movement by external magnetic rod on planar surface with 3 designed experiment. First, ferrofluid droplet was controlled movement all along the planar surface. Second, changing angle of surface was adjusted during moving drop on left and right. And third, particle pick-up of powder on gold surface was examined on flat surface.

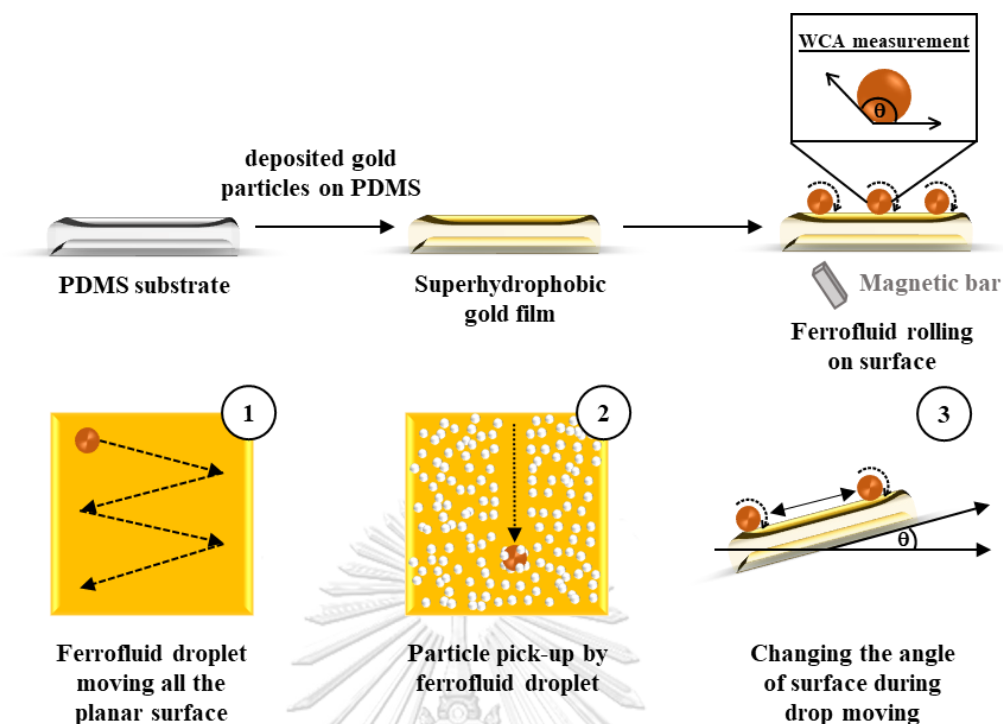


Figure 3. 3 Schematic showed applying magnetowetting on fabricated superhydrophobic surface.

3.6 Detection SERS spectra of PET on fabricated gold film

Another application of fabricated superhydrophobic gold film, it was applied to use as a SERS substrate to detect p-Aminothiophenol (PATP). PATP solution was prepared with 1 mM of concentration in alcohol. PDMS and fabricated gold film at 30 min, 2 h and 4 h were immersed in PATP solution overnight. Then, all films were cleaned excess PATP with alcohol and kept its dried at room temperature. PATP on fabricated gold films were detected by Raman spectrophotometer. SERS signals were received by using 780 nm of the excitation wavelength, 1 mW of the laser power, 50 μm pinhole of the laser aperture, 1 second of the exposure time and 32 scans of the number of exposures.

3.7 Characterizations

The morphological structure of gold film was characterized by Scanning Electron Microscope (SEM, JEOL JSM-6510A) operated at 20 kV under high vacuum mode. The elemental analysis of the generated gold film was performed using Energy Dispersive X-Ray Spectroscopy (EDX). Wettability of gold film on PDMS substrate was evaluated by using Water contact angle (WCA) measured by in-house goniometer. To obtain WCA, the digital images of 2 μ L DI water were captured by Nikon D90 digital camera with Macro lens. LED light source (YN 600 Pro LED) with diffuser filter was placed at the backside of droplet in order to gain the highest contrast between droplet and background. The captured image was transferred to the ImageJ program (developed at the National Institutes of Health and the Laboratory for Optical and Computational Instrumentation) with Dropsnake plugin⁶³⁻⁶⁶ for calculating WCA. The results of WCA from in-house goniometer weren't significantly different when compared with standard goniometer (rame'hart instrument 200-F1) (showed in table 3.1) X-ray diffraction patterns of PDMS and gold film at different deposition time were collected by X-ray diffractometer (Rigaku Model: D/Max-2200) with a scan rate of 0.02 deg/min, using Cu Ka irradiation (0.154 nm, 40 kV, 30 mA). The functional groups of PDMS and gold film on PDMS at different deposition time was characterized by infrared spectrophotometer (Thermo scientific Nicolet iS5) UV-Visible spectrophotometer was investigated spectrum of gold particles on PDMS at different deposition time.

Tabel 3. 1 Comparison of Water contact angle measurement between standard goniometer and in-house goniometer on bared PDMS and gold film on PDMS.

Sample	Instruments	Mean of WCA (degree)	SD	P-value
Virgin PDMS	standard goniometer	113.66	0.50	0.10
	in-house goniometer	111.20	2.96	
Gold film on PDMS	standard goniometer	150.46	13.75	0.53
	in-house goniometer	154.51	1.39	



CHAPTER 4

RESULTS AND DISCUSSION

4.1 Substrates for fabrication superhydrophobic gold film

Gold films were fabricated on 3 different types of substrate which were glass slide, acrylic and polydimethylsiloxane (PDMS). Substrates were cut in square shape without any treatment on the surface. For fabrication of gold film, gold growth solution (AuGS) was dropped in 200 μL on substrates. Then, the substrates with AuGS were left undisturbed about 4 h at room temperature condition. After deposition reaction finished, gold films were washed by DI water, dried in vacuum chamber and then, gold films with circle shape were received on glass slide, acrylic and PDMS in Figure 4.1(A2,B2,C2). All gold films were investigated wettability on the surface by measuring WCA (Figure 4.1G). WCA of gold films on glass slide and acrylic were about 133° and 138° respectively but WCA of gold film on PDMS was up to 154° which meant it had a superhydrophobic property on the gold film surface. Therefore, PDMS was chosen to be a substrate for this work.

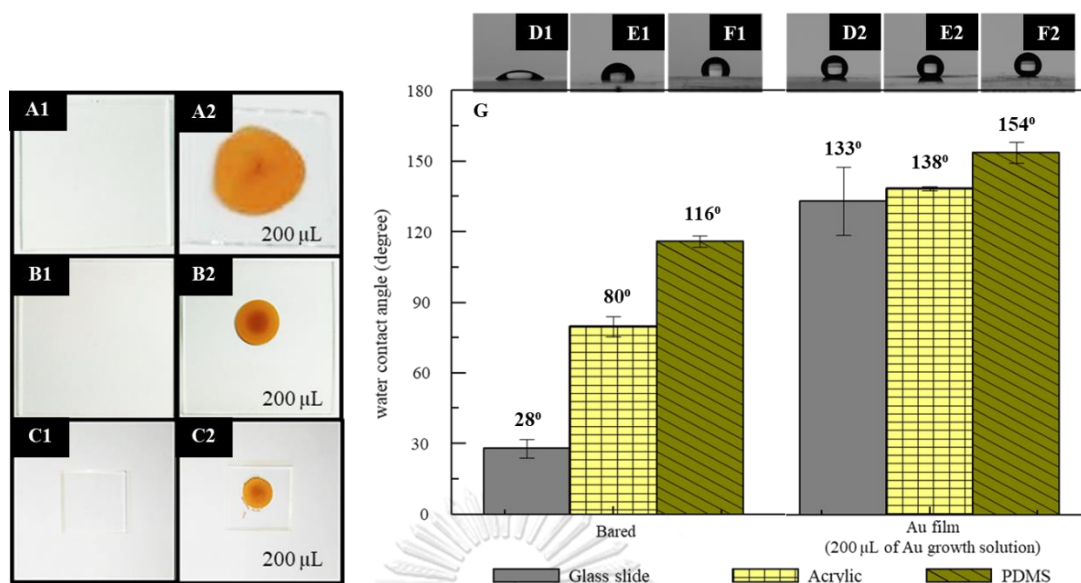
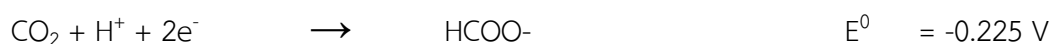
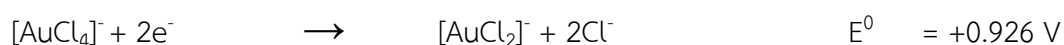
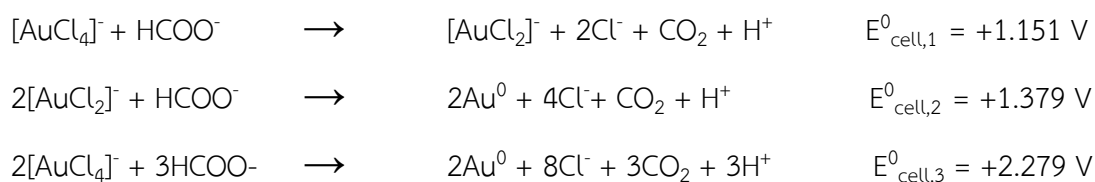


Figure 4. 1 Images of substrates, gold film with 200 μL of AUGS and: glass slide(A1, A2), acrylic(B1, B2) and PDMS(C1,C2), images of water droplet on bared substrates and gold films on substrates: glass slide (D1,D2), acrylic (E1,E2) and PDMS (F1,F2) and graph showed WCA on bared substrates and gold films on each substrate(G)

4.2 Fabrication of gold film on PDMS

In the study, gold microstructures were fabricated by one-pot synthesis using a chemical reaction between chloroauric acid (HAuCl_4) and sodium formate (HCOONa) which acts as metal ion sources and reducing agent, respectively at room temperature. From redox reactions, the generation of gold particles (Au^0) is spontaneous reaction due to the positive value of $E^0_{\text{cell},3}$. From the final reaction, there is no chemical residual left on the surface of gold particles because only protons with chloride ions and carbon dioxide gas are byproducts of the reaction.





The generation of gold particles was monitored by using laser beams irradiated through the solution with the transparent PDMS substrate was laid at the bottom of the holder as shown in Figure 4.2. The appearance of laser beams for investigation of tyndall effect in solution and color changes of PDMS substrate are evidences to reveal the existence of gold particles. The formation pathway of gold particles is discussed based on the reduction potential. At the first stage, the reduction reaction of $[\text{AuCl}_4]^-$ into Au^0 are proposed that $[\text{AuCl}_4]^-$ is possibly reduced to either $[\text{AuCl}_2]^-$ or Au^0 according to the positive reduction potential⁶⁷. These species undergo by rapid electron transfer process which $[\text{AuCl}_2]^-$, Au^0 and CO_2 are produced. However, the sodium formate is a mild reducing agent and it is rather formed as formic acid in acidic condition, therefore, the reaction proceeds efficiently by firstly reduced $[\text{AuCl}_4]^-$ to $[\text{AuCl}_2]^-$ ⁶⁷. Then electron transfer occurs to produce Au^0 and CO_2 . This phenomenon could be proved by investigating the color changes the gold growth solution. At initial stage (0 - 20 min), the solution was in clear yellow pale solution representing the characteristic color of $[\text{AuCl}_4]^-$ and the PDMS substrate was still transparent. The yellow of the solution began to decrease after 20 minutes. This observation suggests that the species of $[\text{AuCl}_4]^-$ decreases which express that the reduction of $[\text{AuCl}_4]^-$ (yellow) to $[\text{AuCl}_2]^-$ (colorless) is favorable. However, the laser beam on solutions was clearly observed when the reaction was prolonged for 40 minutes with the solution color changes from yellow to violet. In this stage, $[\text{AuCl}_4]^-$ and $[\text{AuCl}_2]^-$ are reduced into Au^0 atoms which later form nucleation of nanoparticles spread all over the solution. Due to La Mer model⁶⁸, the nucleation is moved to the growth (aggregation) process to reduce the surface energy of the system, therefore,

the nanoparticles were formed when the time reached 100 minutes then gold color on holder appeared.

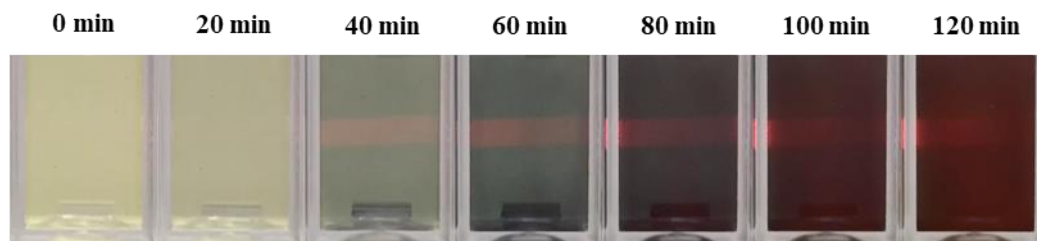


Figure 4. 2 Time lapse of growth solution with laser radiation (A) from 0-2 h with interval of 20 minutes.

In previous studies^{44, 69, 70}, most of the works used the method by incubating a substrate in the growth solution. The method provided the uniform pattern of the generated gold film. However, an enormous amount of the excess AuGS after the reaction obtained. To design different patterns of gold films on the substrate, this might involve the complicated step to architect the pattern on the substrate. To reduce these weaknesses, the method for in-situ self-assembly of the gold microparticles was applied on the free surface of PDMS using different volumes of the AuGS in order to determine the versatility of the proposed method. The AuGS stock solution was freshly prepared by mixing the solution of $[\text{AuCl}_4]^-$ and HCOO^- . The mole ratio of $[\text{AuCl}_4]^-$ and HCOO^- were optimized in order to obtain the smooth and uniform gold film (Figure 4.3). The concentration of HCOONa was changed to examine and fabricate the proper gold film which were 0.2, 1 and 5 M. In term of hydrophobicity measured by water contact angle, the appropriate ratio (give the maximum contract angle $\sim 159^\circ$) is determined at 1:80 which will be used in further experiments across this manuscript.

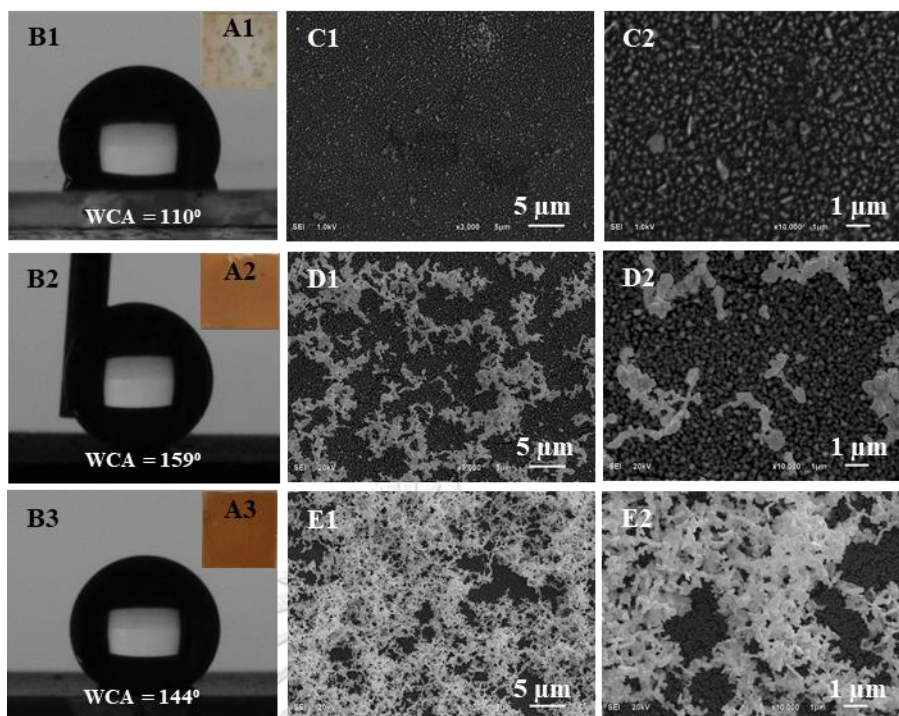


Figure 4. 3 Pictures of gold film, droplet of DI water and WCA and SEM images from the reaction between $[AuCl_4]^-$ and $HCOONa$ at different concentration of $HCOONa$: 0.2 M (A1, B1, C1-C2), 1 M (A2, B2, D1-D2) and 5 M (A3, B3, E1-E2) respectively.

In this section, the relative between volume of gold growth solution, radius of gold film and morphology were investigated. Moreover, to confirm production of pure gold particles on gold film, the proportion of chemical elements was detected using EDX. Gold film was fabricated on a free standing PDMS substrate by varying volume of the gold growth solution from 50 – 1,000 μ L. A drop of gold growth solution spread equally on the PDMS surface and circle shape of gold film was obtained. Under prevented evaporation condition during the reaction, gold films were received with homogeneous surface and the coffee ring effect was not observed as shown in Figure 4.4A. When the reaction was incubated for 4 hours, the solid gold color on the substrate was noticed instead of purple originated from plasmonic phenomenon of gold nanoparticles. This suggests that gold film was produced by self-assembly of gold particles in microscale and fully covers the

PDMS surface. Relationship between volume of gold growth solution and area of gold film was investigated as shown in Figure 4.4B. It can be seen that the area of gold film was linearly related to dropped volume (with slope of 1.17).

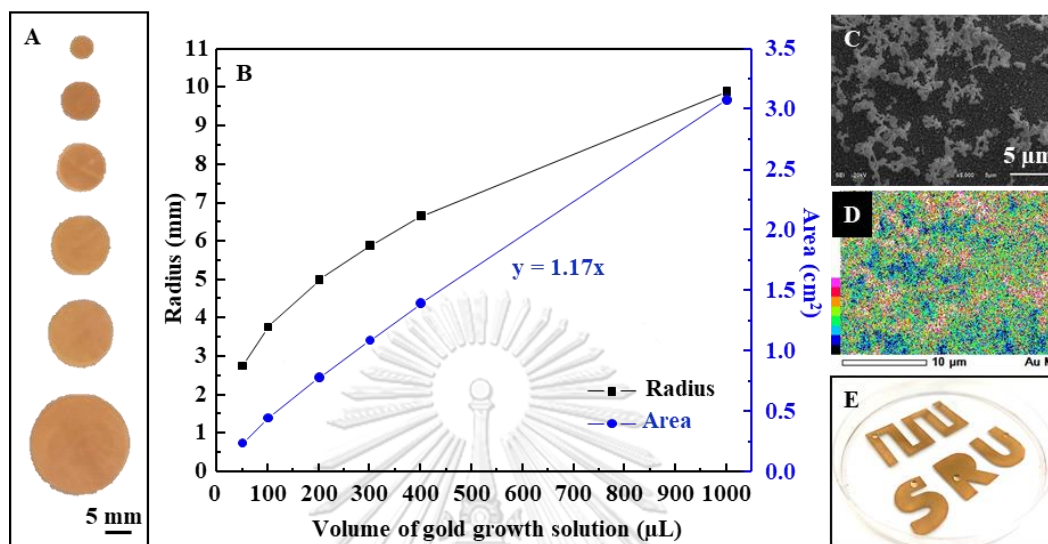


Figure 4. 4 Images of gold film on free surface PDMS in different volume of AuGS (A): 50, 100, 200, 300, 400 and 1,000 μL (left-right), graph shows the relative between volume of gold growth solution and radius or area of gold films (B), SEM images of deposited gold particles on PDMS (C), EDX mapping from gold film (D) and gold film in different patterns (E).

After the gold particles deposited on substrate completely, to gain an insight information of gold structure, the morphology of the generated gold film was deeply investigated by using SEM as shown in Figure 4.4C. Figure 4.4C shows the structure of deposited gold microstructure containing at least 2 different layers: First layer was spherical gold particles with homogeneous deposition and second layer was a secondary structure of gold particles. The film on PDMS was composed of gold particles all the surface that was proved by EDS as shown in figure 4.4D. Moreover, the different patterns of gold film with homogeneous and smooth surface was received as shown in Figure 4.4E. This suggests that the area of gold film can be

completely designed by controlling the dropped volume of the AUGS and this method can create the different patterns of gold film

On bottom layer, the gold particles with irregular spherical shape were uniformly deposited on PDMS surface. This suggests there is possibly interaction between gold particles and functional groups of PDMS. Then, the functional groups of gold film at 15 mins and 4 h deposition time and PDMS were characterized and observed the functional group changing by Infrared spectroscopy. IR spectra including the spectrum of bared PDMS, gold film at 15 min and 4 h deposition time and gold film at 4 h deposition time which was removed some part of gold particles is shown in Figure 4.5. The characteristic peaks of PDMS are clearly observed at 2950–2960 cm^{-1} , 1260–1259 cm^{-1} , 1020–1074 cm^{-1} and 789–796 cm^{-1} representing asymmetric CH_3 stretching in Si-CH_3 , CH_3 deformation in Si-CH_3 , Si-O-Si stretching and $-\text{CH}_3$ rocking and Si-C stretching in Si-CH_3 , respectively. In this case, the signal of Si-H group (2154 cm^{-1}) cannot be observed. The pattern of IR peaks from bare PDMS and PDMS of gold film (4h) are robustly similar. The functional groups of PDMS substrate are totally unchanged indicating that the gold particles were generated from only the reduction of HAuCl_4 and formate ions. The generated gold ions/particles might be interacted via electrostatic force with the functional group of Si-O-Si (1020–1074 cm^{-1}) on PDMS. Interestingly, the characteristic IR peaks of the sample with gold film generated for 4 h are completely disappeared. This suggests that the light might not irradiate though the thick gold film to reach the functional group of PDMS. However, there is no IR peaks on the gold film suggesting that the gold film is very clean with no chemical residuals after deposition process.

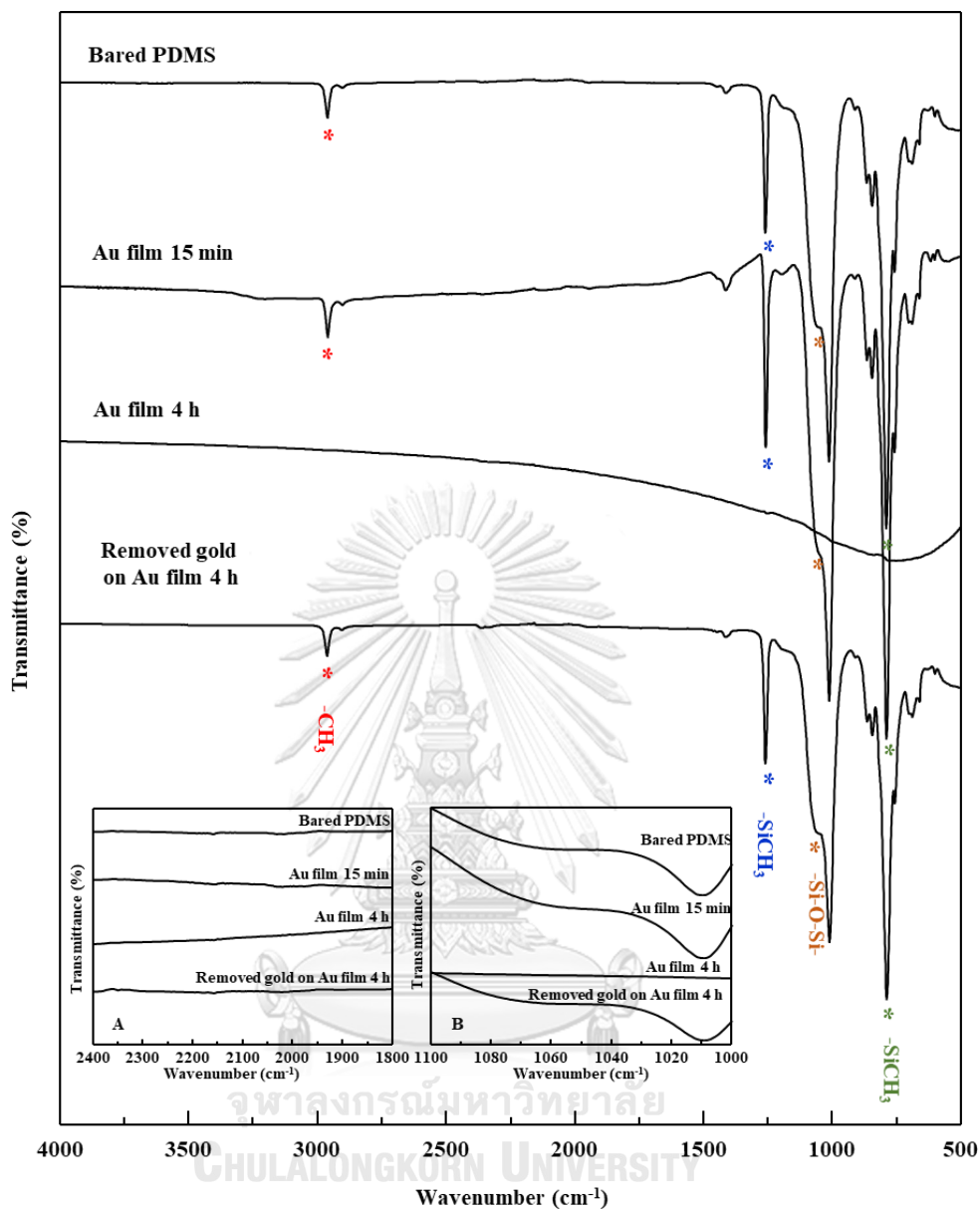


Figure 4. 5 IR spectrum of bared PDMS and Au film at 15 min and 4 h deposition time and Au film at 4 h deposition time with removed some gold particles on the surface.

The second layer involved the deposition process based on the self-assembly of individual gold microparticles into secondary structure. Interestingly, the size and shape of gold particles on first layer are totally different from the gold particles in secondary structure on the second layer. This observed phenomenon and

mechanistic study of the deposition of Au microparticles onto the PDMS substrate will be discussed in the later section. The elemental analysis of gold film was performed by using SEM-EDX as shown in Figure 4.4D. It could be seen that only pure gold particles were observed on EDS mapping suggesting that showed 58.24% atom of Au, 26.88% atom of Si from PDMS substrate and the other elemental fractions were in a few amounts of C and O atom (Figure 4.6).

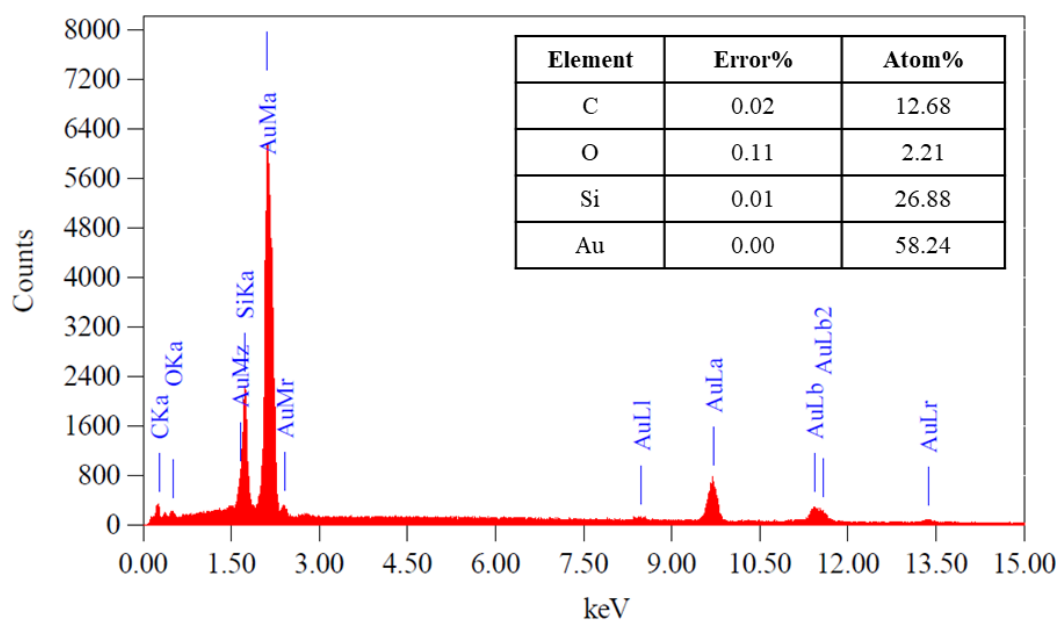


Figure 4. 6 EDX pattern and percent atom of elements obtains from the fabricated gold film at 4 h deposition time.

Moreover, to confirm the crystalline structure of gold particles on film, XRD pattern of gold film at different deposition time showed the spectra at 111, 200, 220, 311 and 222 that is a pattern of XRD spectra of face-center cubic gold particle^{71, 72} as shown in Figure 4.7. At 30 min deposition time of gold film, it could observe the pattern of PDMS because the gold particles were deposited for the first layer and PDMS surface was not completely filled with gold particles. For the gold film at 2 and 4 h deposition time, XRD pattern showed the sharp peaks of gold particles with face-center cubic structure.

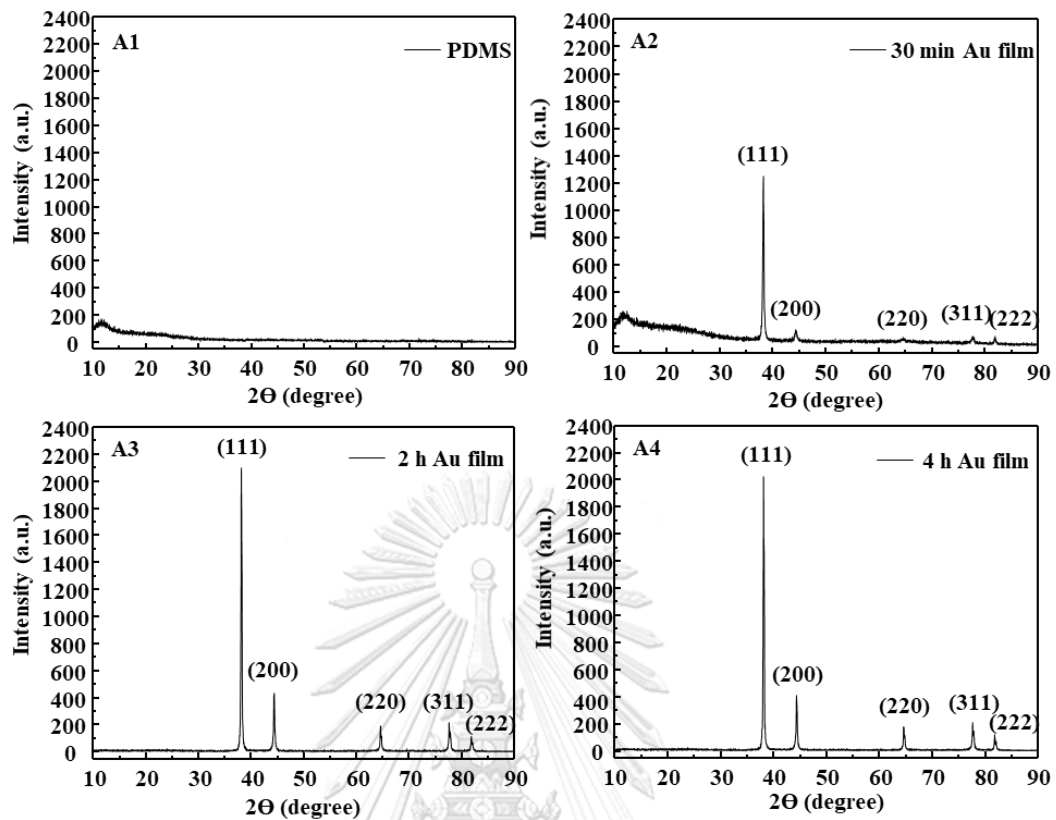


Figure 4.7 XRD pattern of PDMS (A1) and fabricated gold film at different deposition time: 30 min (A2), 2 h (A3) and 4 h (A4).

The average crystallite size of gold (d) was calculated in Table 4.1 by using Debye-Scherrer formula in Eq.7

$$d = \frac{K\lambda}{\beta \cos\theta} \quad \text{Eq.7}$$

In Debye-Scherrer formula, K is normally valued as 0.89, λ is wavelength of X-ray radiation source which is Cu source with 0.154 nm, β is referred to the width at half maximum height of spectrum and θ is come from 2theta of XRD spectrum.

From the table, it can be seen that the estimated size of particles was slightly increased due to the early stage of the deposition time, while the estimated size of particles was steady after 2 h of deposition time. This suggests that the particles were initially grown in the first stage as the crystal size was slightly increased.

However, the grown rate was stopped after 2 h of prolonged reaction because the size was rarely changed. The observations suggest that the particles tends to aggregate and to form as secondary structures. These results are in good agreement with SEM images of the gold films as shown in Figure 4.4C.

Table 4. 1 Calculated average crystallite size of gold particles from of gold film at different deposition time by using Debye-Scherrer formula.

diameter (nm)	111	200	220	311
30 min	33	24	63	39
2 h	38	35	49	51
4 h	39	36	59	43

4.2 Wettability of the gold film

From the previous section, uniform gold films were successfully fabricated on PDMS surface. In this section, wettability and morphological structures of the generated gold film at different deposition times (15 min – 24 hours) was deeply investigated as shown in Figure 4.8.

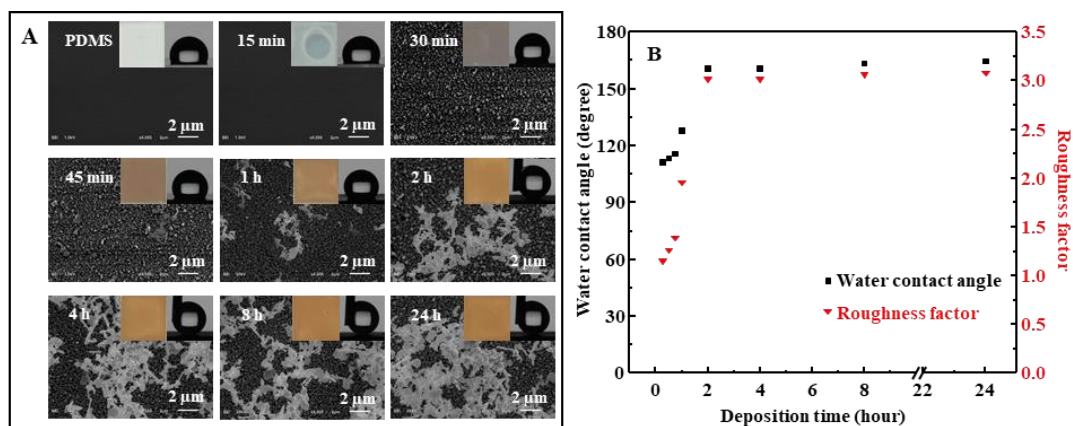


Figure 4.8 Optical images, pictures of water droplet and SEM images of fabricated gold film on $0.5 \times 0.5 \text{ cm}^2$ PDMS at different deposition time (A) and graph shows relative between WCA or roughness factor calculated using Wenzel's equation and deposition time (B) from 15 min-24 h (WCA on virgin PDMS = 108°)

It could be seen that the color of gold film initially appeared in purple after 30 min of the deposition time and changed to gold color when the deposition time longer than 45 min. The color of gold film reflects to the size and density of gold particles deposited on the surface. To obtain insight information of size of gold particles, the UV-visible spectroscopic technique was performed on the gold films at every deposition time with transmission mode. From UV-visible spectra (Figure 4.9), the gold film at 30 min exhibits plasmon band at around 500-600 nm^{73, 74}. The intensity of the plasmon band of fabricated gold film increased with the baseline shift when the deposition time increased. This suggests that the amount of gold particles was increasingly deposited on the substrate and certainly thicker. However, only baseline shifted without any plasmonic band when the deposition time was longer than 30 min. This suggests that gold film had multilayer deposition of gold particles with the size in micrometer scale.

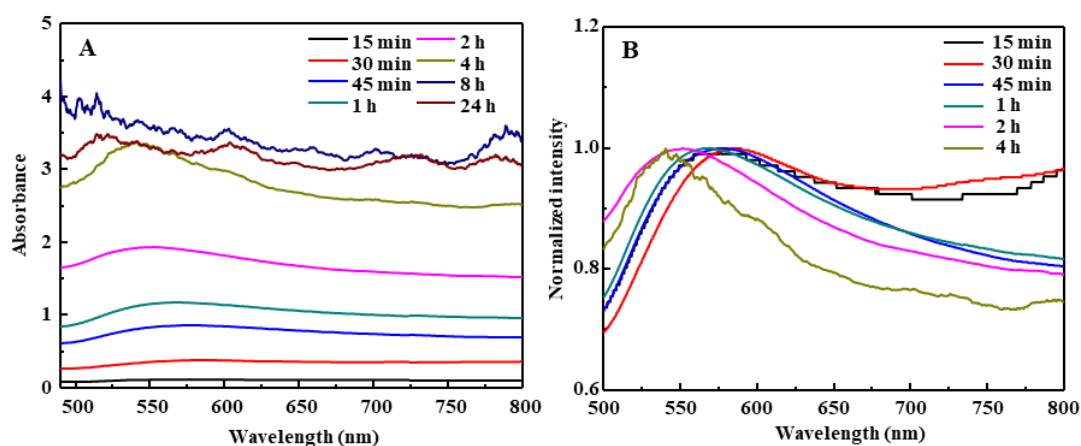


Figure 4.9 Raw UV-Vis spectrum of fabricated gold film at different deposition time from 15 min-24 h and normalized UV-Vis spectrum of gold film at different deposition time from 15 min-4 h.

To obtain the hydrophobicity of the generated gold films, a droplet of 2 μL of DI water on the gold films were captured. The WCA was measured by Image J program with dropsnake plugin⁶³⁻⁶⁶. Figure 4.8B show the relationship between WCA and the deposition times. The WCA was changed in 3 significant steps. In the first step (15mins-45mins), the WCA of gold films was approximately 112° – 116° which are close to the WCA of virgin PDMS (108°)^{75, 76}. In this stage, we observed the color of the film are in purple with plasmonic band at 500 –600 nm but the WCA was not different from using virgin PDMS. This suggests that only the nucleation of small gold particles in nanoscale were produced and the deposition of the generated seed of gold particles were induced by the silane group (Si-H) of PDMS surface to form a first layer. This size of the deposited gold particles might not affect the original roughness of the surface. Therefore, the WCA were just slightly changed. For the second stage (45min – 2 h), the WCA were dramatically increased from 116° to 161° . The gold film with superhydrophobic property was obtained when the deposition time was reached 2 hours. From SEM images, it can be seen that the first layer was fully covered by gold microparticles with the secondary structures formed as second

layer. This phenomenon reflects to the color of gold film which express in gold color. The secondary micro/nanostructure in combination with low surface energy the PDMS substrate might be a perfect model for the development of superhydrophobic surfaces because the roughness of the surface was dramatically increased and acts as lotus leaf effects. After 2 h of deposition, the WCA slightly changed from 161° to 164° because the reaction was finished by consuming all Au^{3+} ions and most of the generated gold particles were already deposited on substrate. It can be seen that SEM micrographs of the gold film were insignificantly changed. (showed in Table 4.2). These observations revealed that superhydrophobic gold film was obtained after using deposition time at least 2 hours. The satisfied model to describe superhydrophobicity of the fabricated gold film was examined using either Wenzel's model⁵³ or Cassie-Baxter's model⁵⁴. These models can be determined by using the roughness factor (r) of the surface which can be calculated by a following Eq.8.



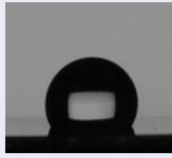
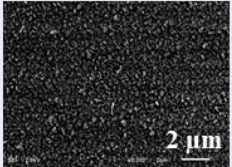
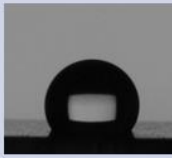
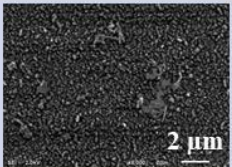
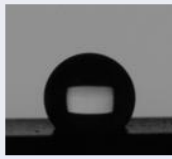
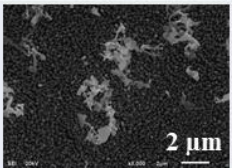

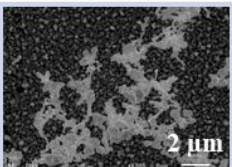

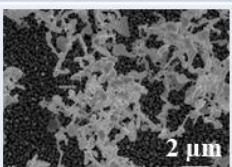
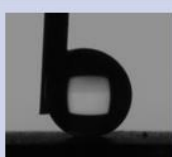
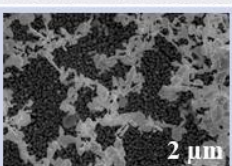

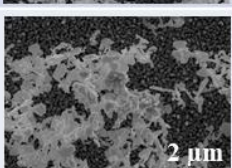
$$\cos \theta^* = r \cos \theta^E \quad \text{Eq.8}$$

The θ^* is referred to the apparent contact angle of a target surface and θ^E is an equilibrium contact angle for the ideal flat surface (a virgin PDMS in this case). The roughness factor (r) is the ratio between real surface area and projected surface area, therefore r is always more than 1 for a rough surface. The higher roughness surface, the higher r value obtains. Roughness of the surface generally enhances hydrophobicity of the corresponding flat surface. The roughness factor r between 1-1.7 will be underlying on a basic assumption Wenzel's model. However, the switching from the Wenzel to the Cassie-Baxter state will occur when r exceeds 1.7^{52, 77}. The behavior of a liquid drop on a rough surface was changed from penetrating into the spikes (Wenzel state) to suspend on the spikes (Cassie-Baxter state) reflecting to the wetting phenomenon of the superhydrophobic surface. The

calculated roughness of the gold film was plotted against the deposition time to investigate the wetting phenomenon of the surface as shown in Figure 4.8B.

Strong correlation between roughness and WCA was observed. Using deposition time in range of 15-45 mins, the roughness was in between 1.15-1.38 indicating that the water droplet penetrates on the surface based on Wenzel state. At this stage, the contact angle and its hysteresis increase as the roughness factor increases for the hydrophobic surface. From SEM images, the gold particles were initially deposited on PDMS surface with uniform distribution. This roughness was not sufficient to create the suspension state of a water droplet. However, the roughness increased to 1.96 and was up to 3.02 after 2 hours of deposition time when the secondary structures were generated on the first layer of gold microparticles. Enhancing of the air fractions on the surface induced the suspension of water droplet based on Cassie-Baxter's model. This reflects the increasing of WCA from 116° to 161° . After 2 hours, the roughness slightly changed because the reaction was almost accomplished because of the limitation of chloroauric acid in the solution. It is in good agreement with SEM images from 2 to 24 h.

Table 4. 2 WCA, calculated roughness factor from Wenzel's theory, pictures of 2 μL DI water on 0.5x0.5 cm^2 gold film and SEM images of morphology on gold film surface at different deposition time

Time	WCA (degree)	Roughness factor	Pictures of droplet	SEM images
15 min	111	1.15		
30 min	113	1.26		
45 min	116	1.38		
1 h	128	1.96		
2 h	161	3.02		
4 h	160	3.01		
8 h	163	3.06		
24 h	164	3.08		

To confirm the model of superhydrophobic gold film, the dynamic contact angle involving advancing angle (θ_a) and receding angle (θ_r) of droplet on superhydrophobic gold film was measured. The hysteresis (H) is calculated from the difference between the angles ($H = \theta_a - \theta_r$). If it is lower than 10° , the surface is claimed as a non-wetting surface. The result showed in Figure 4.10 the pictures of droplet in advancing angle and receding angle were not obviously different and the hysteresis was 2° which was less than 10° so our method can fabricate the gold film to be a non-wetting surface with high WCA.

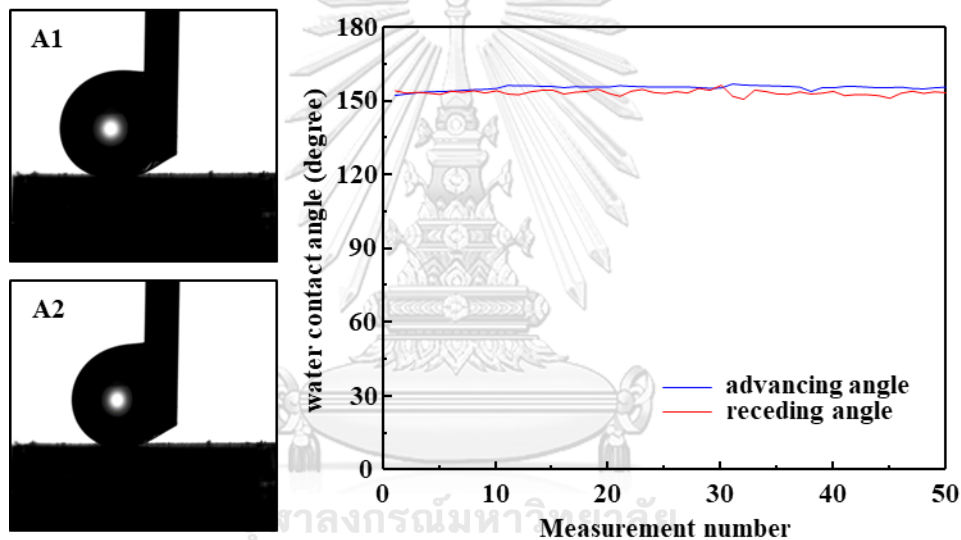


Figure 4. 10 Pictures of water droplet on the gold film for measuring dynamic CA: advancing way (A1) and receding way (A2) and graph shows the WCA of advancing and receding angle during the measurement time (B).

4.3 Deposition mechanism of gold particles on PDMS

In the previous section, the fabrication of superhydrophobic gold film on PDMS was revealed. The wettability of the gold films can be controlled by the deposition time. The morphological structure of the gold films has strongly influent to the superhydrophobicity especially the secondary structure of gold microparticles. In the section, the mechanism of the generated gold microstructures deposited on

PDMS surface has been deeply investigated. Figure 4.11 shows SEM images of superhydrophobic gold film containing two layers of gold particles deposition. It is clearly seen that there are 2 layers of gold microstructure on the PDMS substrate.

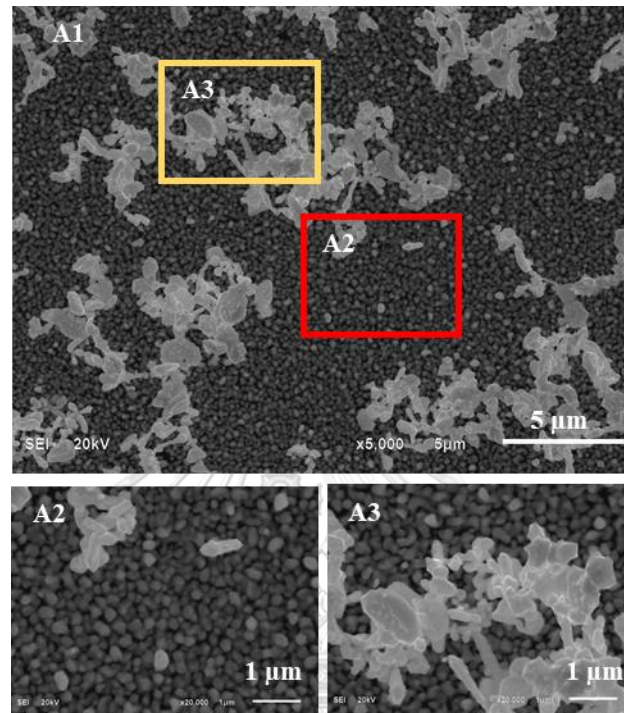


Figure 4. 11 SEM images show the structure of deposited gold particles (A1) on the PDMS: gold particles on the first layer (A2) and secondary structure (A3)

On the first layer (Figure 4.11A2), the gold particles with spherical shape were uniformly deposited on the PDMS surface. To investigate the growth rate of the particles, size of gold particles on the layer was measured and counted for each of deposition time as shown in Figure 4.12. The results showed the gold particles size with the first coverage started at 130 nm, increased to 215 nm after 2 h and slightly enlarged the size afterwards (Figure 4.12D1). Until 2 h of deposition, the growth of gold particles couldn't continue enlargement the size because the surface was filled with gold particles. It suggests that the gold particles were initially deposited on PDMS as the particle seeds and then slowly grew when the deposition time was prolonged.

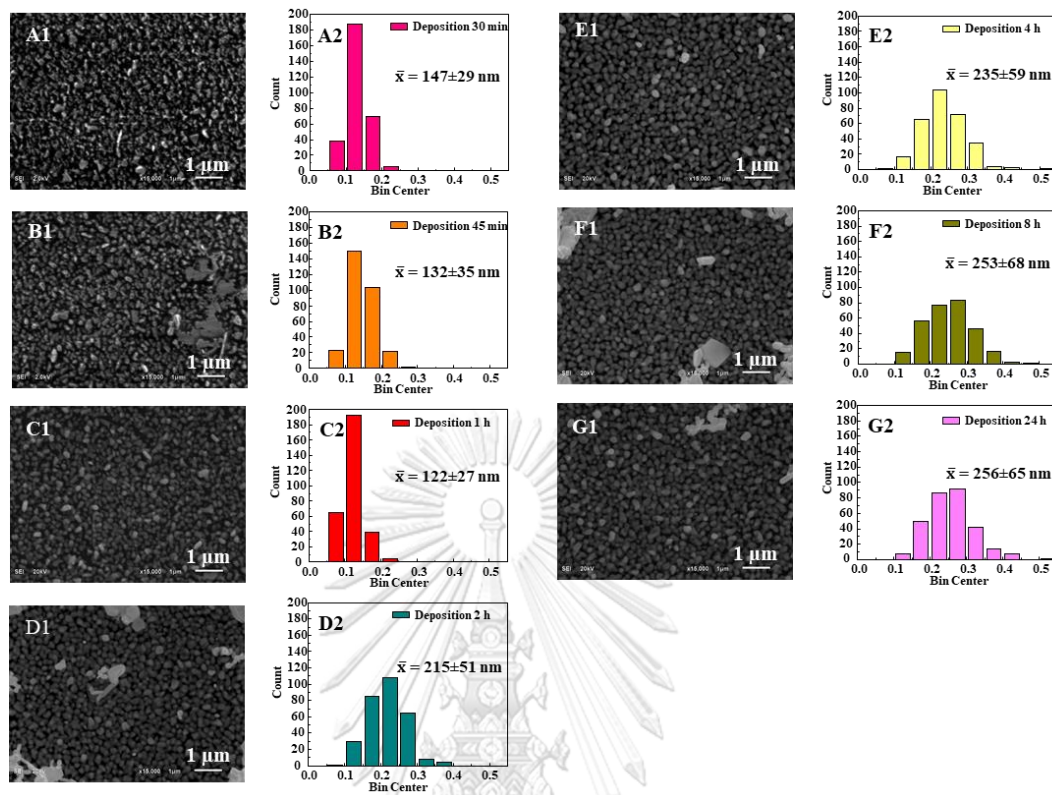


Figure 4. 12 SEM images of gold film on $0.5 \times 0.5 \text{ cm}^2$ PDMS and distribution graph of particle size at different deposition time: 30 min (A1,A2), 45 min (B1,B2), 1 h (C1,C2), 2 h (D1,D2), 4 h (E1,E2), 8 h (F1,F2) and 24 h (G1,G2).

In the case, the excess of gold ions in the solution could be aggregated into another gold structure which was called secondary structure. Both layers of gold particles were deposited uniformly and cover over the whole surface. To investigate the interaction between gold particles and PDMS, the superhydrophobic gold film was sonicated in DI water for 15 min. and then radiated the laser through the solution. In Figure 4.13, the tyndall effect was observed because a beam of laser could clearly appear in the solution. It suggests that the free particles should disperse in the solution. The remain structure of the sonicated gold film and the particles from the solution was monitored by SEM. SEM images show the secondary structure was detached from the surface after sonication but the spherical gold

particles at the first layer was still deposited on the PDMS surface (Figure 4.13A2, 4.13B2). The particles dispersed in the solution after sonication was collected and investigated by using SEM. It can be seen that the particles dispersed in the solution were in the shape of secondary structure. The observation indicates that the spherical gold particles were strongly interacted with PDMS surface. The strong interaction might generate from the electrostatic interaction between Si-O and Au before and after the reduction. However, the secondary structure of gold particles did not directly interact with PDMS surface, but they physically interacted with the first layer of gold particles. The interaction might be very weak as it could be separated by sonication process. However, the deposition mechanism between the gold particle with secondary structure and the spherical gold particles was still unclear.

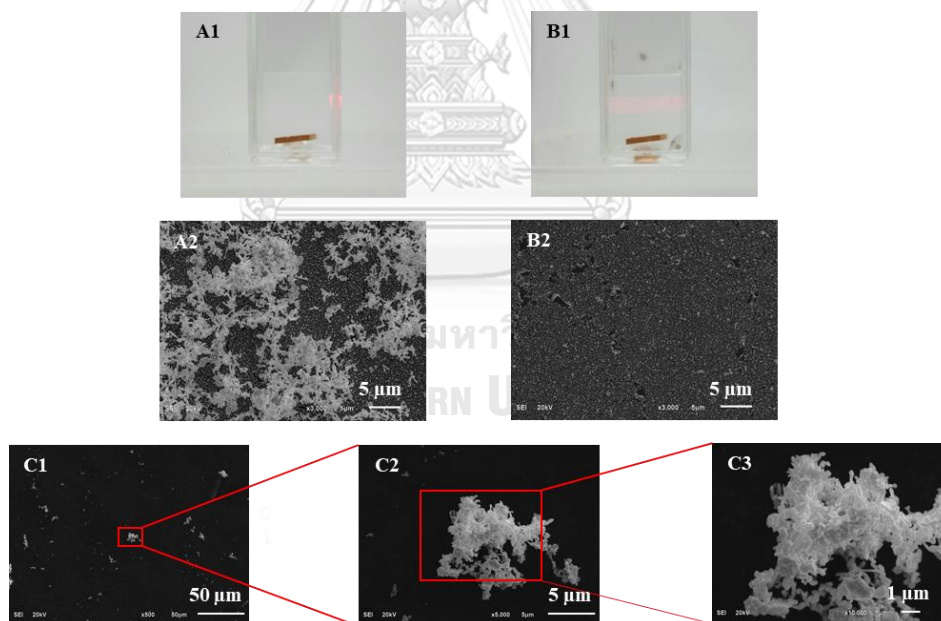


Figure 4. 13 Fabricated gold film in DI water and SEM images before sonication (A1,A2) and after sonication 15 min (B1,B2) and SEM images of sonicated secondary structure from gold film (C1-C3).

To prove how the secondary structure deposited on the first layer surface and the gold particles were attached on the PDMS, the PDMS substrates were placed

in the different position to fabricate the gold film in Figure 4.14. PDMS substrate was placed on the top of AUGS that was against with another PDMS on the bottom. From the experiment, the gold films with different appearance and morphology were obtained. Even though the PDMS was placed on the top of gold growth solution, the spherical gold particles could be deposited as the first layer. The results were in good agreement of the IR spectrum (Figure 4.5). This indicate that some of gold ions (Au^{3+} , Au^+) were induced and mobilize to the PDMS surface by electrostatic force of lone pairs from $-\text{Si-O-Si}-$ group on PDMS. Then the gold ions were reduced by formate ions and growth to form the gold particles on PDMS surface. Due to the strong interaction induced by functional group of PDMS and gold ions, the spherical structures were formed on both positions (top and bottom) with an independent influence from the gravity. However, the secondary structure was occurred only on the PDMS at the bottom position. It could propose that the secondary structure was produced from the excess gold ions in the growth solution and then they were reduced and aggregated to form the complex structure in the solution. Due to gravity force, the gold particles with complex structure were precipitated and deposited on the first layer of the spherical gold particles. Therefore, they only provide a weak interaction on the gold particles of the first layer.

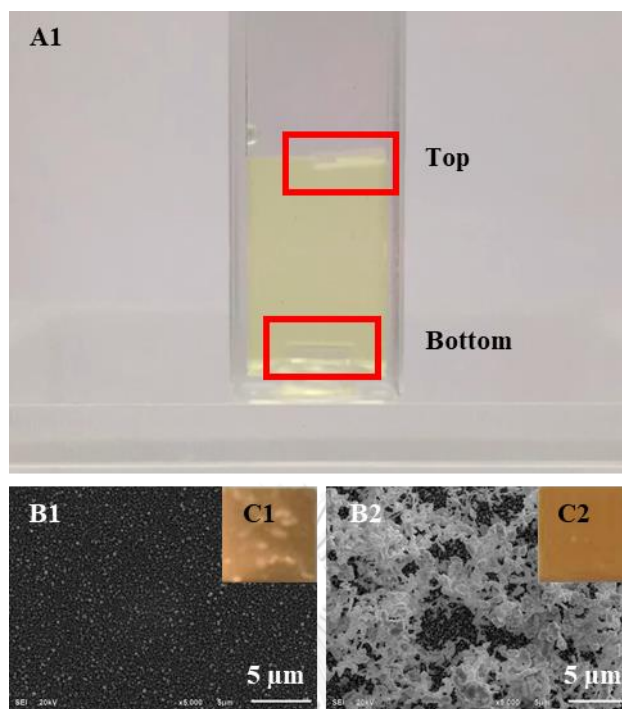


Figure 4. 14 Picture of deposition reaction AuMPs on $0.5 \times 0.5 \text{ cm}^2$ PDMS at the top and bottom of gold growth solution for 2 hours deposition time (A), SEM images and pictures of gold film from the reaction: top position (B1,B2) and bottom position (C1,C2).

Based on investigation of deposition time and the experiments to prove the deposition mechanism of gold film on PDMS, we proposed the deposition mechanism (Figure 4.15) of gold particles on PDMS substrate to form as a superhydrophobic gold film. Firstly, the pathway to reduce Au^{3+} ions into Au^0 by sodium formate which is a mild reducing agent. In this stage, the gold ions (Au^{3+}) should strongly interact with functional group (Si-O-Si) on PDMS surface, then the reduction was occurred to reduce Au^{3+} into Au^+ and Au^0 , respectively. This will generate the spherical gold particles to spread all over the PDMS surface. After the PDMS surface was completely filled with the spherical gold particles, the excess Au^{3+} ions were reduced and aggregated to form the secondary structures. The secondary gold particles were then precipitated on the first layer of gold films by gravity force for being the second layer of gold film. The amount of these structure can be

controlled by only the deposition time and amount of Au^{3+} ions in the growth solution.

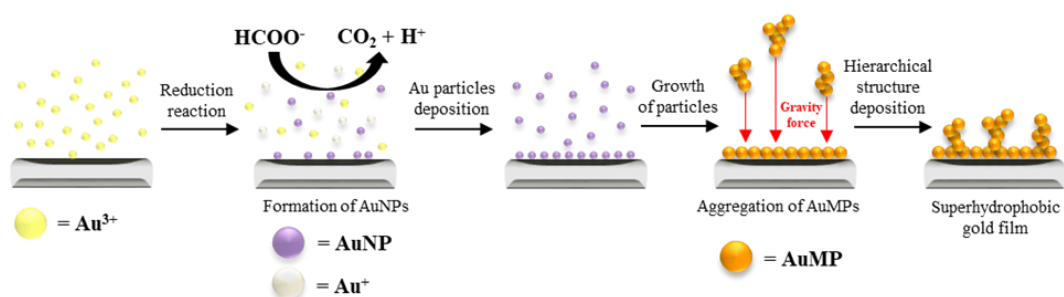


Figure 4. 15 Schematic shows method for fabrication the superhydrophobic gold film on PDMS by reduction reaction between chloroauric acid and sodium formate.

4.4 Stability of non-wetting properties

After the superhydrophobic gold film was clearly investigate, to apply the film for the application, durability should be tested as shown in Figure 4.16. For the experiment that shows in Figure 4.16A, the droplet of water was dropped with a rate 1 drop/1 sec for 2 h at 20 cm height from the gold film that was laid at a 45-degree angle. Every 15 min, the WCA of gold film was measured. The graph in Figure 4.16B shows that the WCA of gold film was not changed significantly after the droplet of water was continually dropping on the surface for 2 h (7,200 drops). The results show that the structure of gold particles on gold film is strongly deposited on PDMS and even though the gold film is used by moving droplet on the surface at least 7,200 times, the gold film still has the superhydrophobic property on the surface.

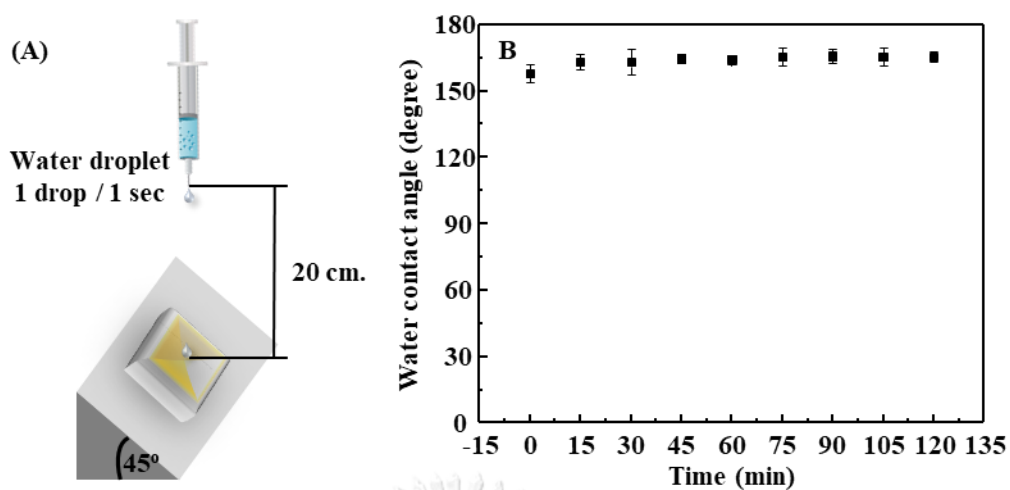


Figure 4. 16 Schematic of durability test of fabricated superhydrophobic gold film by dropping the water at a rate 1 drop/1 sec for 2 h (A) and graph shows WCA of gold film in durability test in every 15 min for 2 h (B).

To confirm the gold film with superhydrophobicity surface, the frame by frame pictures were captured during the droplet were dropping on the surface. From the pictures in Figure 4.17, it shows that droplet jumped on gold film without sticking so the fabricated gold film with this method is a completely non-wetting surface.

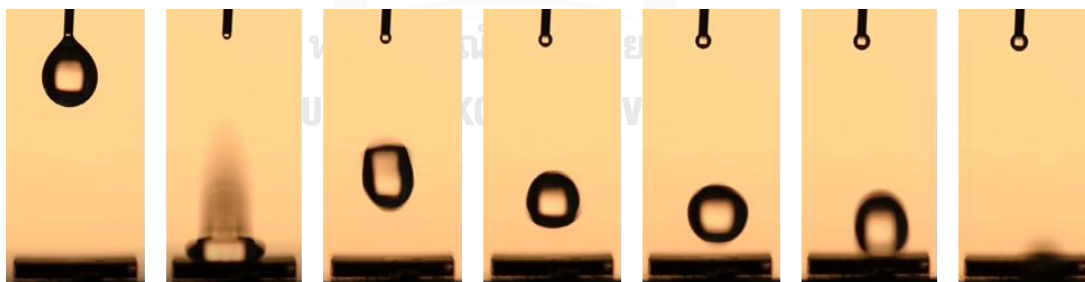


Figure 4. 17 Frame by frame of droplet jumping on non-wetting gold film.

After the superhydrophobic gold films were successfully fabricated, the application of using the films as the substrate to control the droplet by magnetowetting was investigated. Initially, the droplet of 3,000 ppm ferromagnetic solution⁷⁸ was dropped on the surface. The movement of this droplet was controlled

by magnetic stick under the surface. The snapped pictures from the recorded video of the movement of ferromagnetic droplet on over the gold films. The movement of the droplet was tested in every direction all over the surface as shown in Figure 4.18A and Figure 4.18B. The drop was completely moved with no residuals of the liquid left on the surface. This indicates that the gold films are completely express non-wetting surface. Furthermore, the vertical movement of the ferromagnetic droplet was examined by slightly changing the angle of surface as shown in Figure 4.18C. It was found that the droplet can move along the vertical axis with the maximum angle of 13° . It suggests that the movement of ferromagnetic droplet can be performed on the generated gold film in either the horizontal and vertical with 13-degree angle.

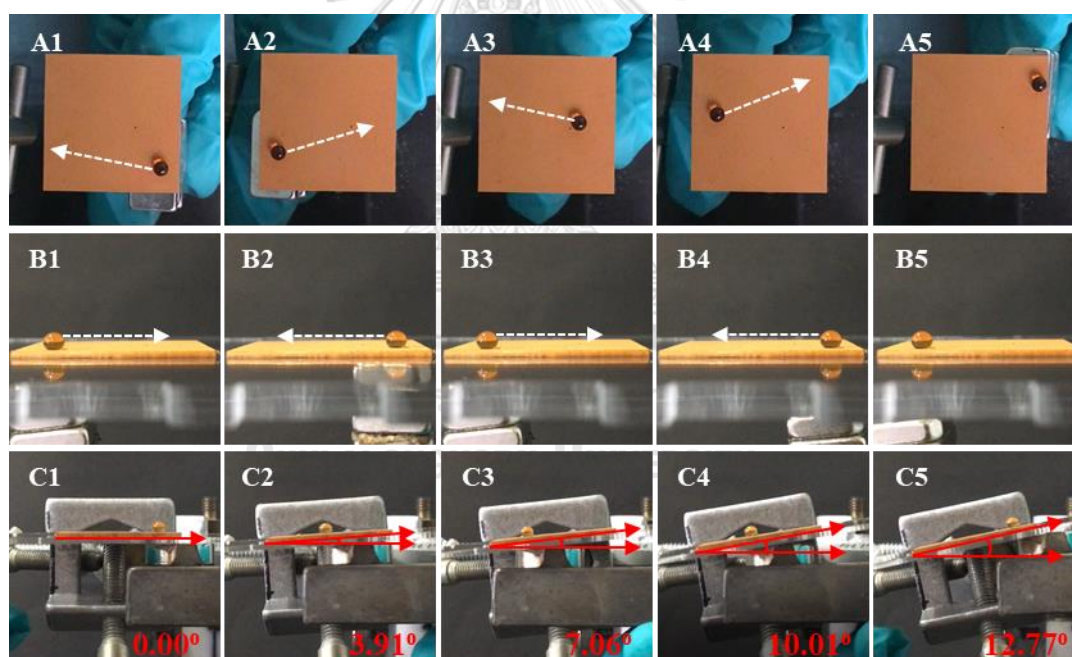


Figure 4. 18 Frame by frame pictures of ferromagnetic droplet moving on superhydrophobic gold film with controlling by magnetic bar: top view (A1-A5) and side view (B1-B5) with horizontal surface and side view with changing the angle of surface (C1-C5)

As this result, the movement of ferromagnetic droplet on non-wetting gold film were studied to use for picking-up particles on the surface as shown in Figure 4.19. the drop could pick the particles during the way of movement and collected them at one point on surface so, this ability can be applied to be a preconcentrate target analyze or a self-cleaning surface.

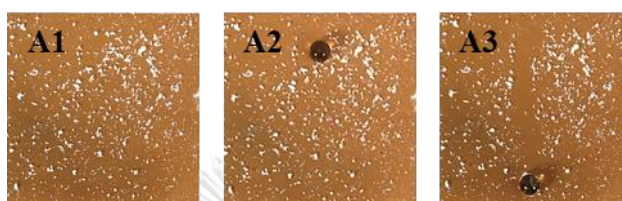


Figure 4. 19 Pictures of ferromagnetic droplet movement to pick up powder on non-wetting gold film.

The pictures of ferromagnetic droplet when it moves on non-wetting surface with controlling movement by magnetic bar were captures as shown in Figure 4.20. During the droplet moves, the WCA on the left and right side of ferromagnetic droplet was monitored as shown in Table 4.3. The results expressed that every positions of droplet gave the similar of average WCA values. The WCA values on left and right side of the droplet were not significantly different with only ~ 4.36 degrees in every position. This observation suggests that the droplet can retain its formation and freely moves on surface. So, this property on surface can be further applied in microfluidic process because the droplet can freely move with no-tail and without laminar flow in the system.

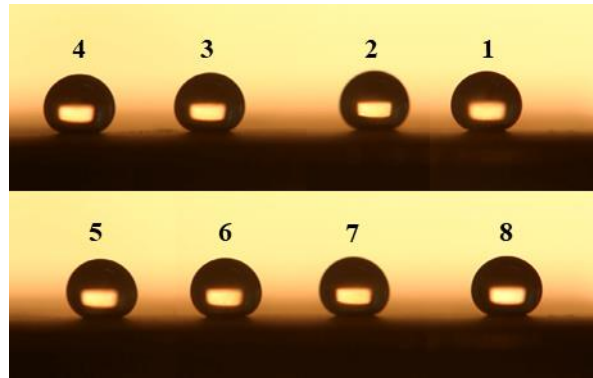


Figure 4. 20 Frame by frame of ferromagnetic droplet moving on non-wetting gold film in different position.

Table 4. 3 WCA-Left, WCA-Right, WCA average and difference between WCA-Left and WCA-Right of ferromagnetic droplet on non-wetting gold film in different position.

Droplet no.	WCA-Left (degree)	WCA-Right (degree)	Avg WCA (degree)	Δ WCA (degree)
1	166	163	164	3
2	165	164	165	1
3	168	159	164	9
4	167	161	164	6
5	160	164	162	4
6	161	168	164	7
7	163	167	165	4
8	165	168	166	3

Due to the morphology of the gold films generated from the gold microstructure, another potential application of the non-wetting gold film is to be used as the powerful SERS substrate. The fabricated gold films at different deposition times at 30 min, 2 h and 4 h respectively were applied as SERS substrates. The efficiency of these substrates was evaluated by using para-aminonitrophenol (PATP) as a probe molecule. The SERS spectra were shown in Figure 4.21. From the result, the characteristic peaks of PATP were clearly observed at 1076 cm^{-1} , 1142 cm^{-1} , 1389 cm^{-1} , 1432 cm^{-1} and 1577 cm^{-1} representing CS stretching, CH bending, CH rocking and CC stretching, CC stretching and CH bending, CC stretching respectively. The intensity of PATP acquired from the substrate with only 30 min of the deposition time shows the highest intensity compared with the other substrates. It represented that fabricated gold film at 30 min deposition time created the appropriate hot spots and could enhance the Raman signal of PATP. The results are in good agreement with the SEM images of gold film at deposition time of 30 min which shows only the first layer of homogeneous spherical gold particles on PDMS. In the part of gold films at 2 h and 4 h deposition time, they showed the lower intensity because the secondary structure of gold microparticles covers the hot spots. Moreover, the variation of Raman intensity across the gold film was investigated by using the 2D spectrum of a peak 1076 cm^{-1} . It was found that the variation of the Raman signals is small across the detection area especially the gold film generated with deposition time of 30 min. This indicates that the hot spots are uniformly distributed across the surface and the relative standard deviation of the detection area is in the acceptable range.

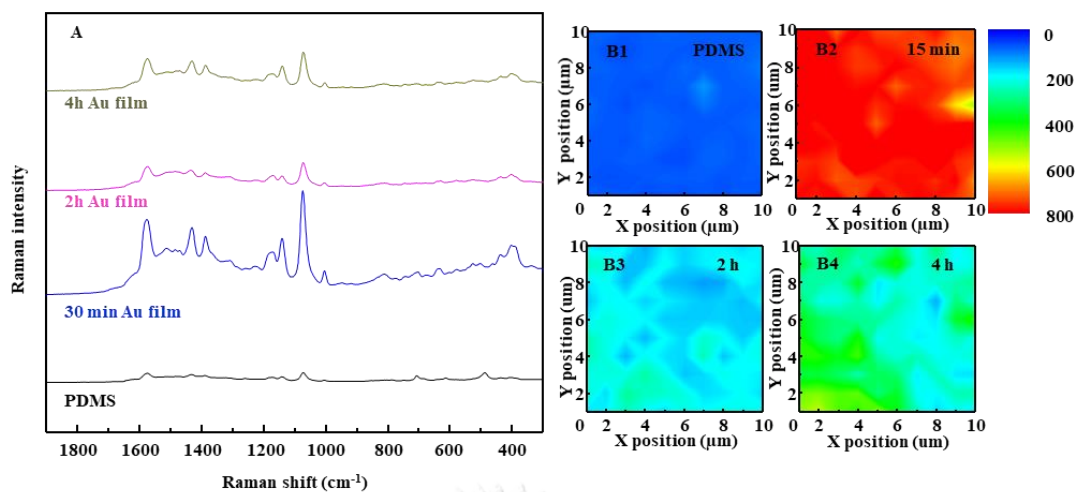


Figure 4. 21 SERS spectrum of PATP on PDMS and fabricated gold film at different deposition time: 30 min, 2 h and 4 h (A) and 2D-Raman Spectrum of PATP on PDMS (B1), fabricated gold film at 30 min (B2), 2 h (B3) and 4 h (B4).

From these applications, it can be concluded that the fabricated gold films can play the dual function as non-wetting surface to control the droplet by magnetowetting and a powerful SERS substrate. The adjustment of the deposition time is only one factors to control the surface for each application. To be use as a SERS substrate, the hot spot of the spherical gold particles is required, therefore, the rapid deposition time was used to obtain the appropriate gold film. On the other hand, the prolonged deposition time was required in order to generate the secondary structure of gold microstructure. These structures provide non-wetting surface to be used as the substrate for magnetowetting.

CHAPTER 5

CONCLUSIONS

In summary, superhydrophobic gold film were successfully fabricated by a spontaneous reduction reaction between chloroauric acid (HAuCl_4) and sodium formate (HCOONa) at ambient condition. The relationship between deposition time and wettability of the fabricated gold films was investigated. It was found that superhydrophobic property were obtained when deposition time reached to 2 h with $\text{WCA} > 160^\circ$ with low contact angle hysteresis ($H=1.93^\circ$). Several characterizations were performed to reveal physical and chemical properties of the gold films. EDS showed that the gold film composed only gold substance with no other elements on the surface. XRD expresses that the film generated with particle in fcc orientation. SEM images revealed the morphology of gold film which contains 2 different layers on PDMS substrate. Spherical gold particles were uniformly distributed over PDMS surface as the first layer and the secondary structure were deposited to form as a second layer. The secondary structure is a main factor to acquire roughness and create superhydrophobic property. Fabricated gold film has durability after 7,200 water-drop testing without losing their superhydrophobic properties These gold films were used as a substrate of magnetowetting. It demonstrated that ferromagnetic droplet can move freely with no-tail and droplet can pick up particles on surface. The fabricated gold films have potential to be used in microfluidic process in order to move the solution without using high pressure pump. Furthermore, they can be used as a powerful SERS substrate to detect chemicals with low concentration (PATP in the case).

REFERENCES

1. Ma, M.; Hill, R. M. Superhydrophobic Surfaces. *Curr. Opin. Colloid. Interface. Sci.* **2006**, *11* (4), 193-202.
2. Quere, D. Rough Ideas on Wetting. *Physica A.* **2002**, *313*, 32-46.
3. Feng, L.; Zhang, Y.; Xi, J.; Zhu, Y.; Wang, N.; Xia, F.; Jiang, L. Petal Effect: A Superhydrophobic State with High Adhesive Force. *Langmuir.* **2008**, *24*, 6.
4. Shiu, J. Y.; Kuo, C. W.; Chen, P.; Mou, C. Y. Fabrication of Tunable Superhydrophobic Surfaces by Nanosphere Lithography. *Chem. Mater.* **2004**, *16* (4), 561-564.
5. Singh, A.; Steely, L.; Allcock, H. R. Poly[bis(2,2,2-trifluoroethoxy)phosphazene] Superhydrophobic Nanofibers. *Langmuir.* **2005**, *21* (25), 11604-11607.
6. Zhang, J.; Li, J.; Han, Y. Superhydrophobic PTFE Surfaces by Extension. *Macromol. Rapid. Comm.* **2004**, *25* (11), 1105-1108.
7. Xu, L.; Chen, W.; Mulchandani, A.; Yan, Y. Reversible Conversion of Conducting Polymer Films from Superhydrophobic to Superhydrophilic. *Angew. Chem. Int. Edit.* **2005**, *44* (37), 6009-6012.
8. Yabu, H.; Shimomura, M. Single-Step Fabrication of Transparent Superhydrophobic Porous Polymer Films. *Chem. Mater.* **2005**, *17* (21), 5231-5234.
9. Jin, M.; Feng, X.; Xi, J.; Zhai, J.; Cho, K.; Feng, L.; Jiang, L. Super-Hydrophobic PDMS Surface with Ultra-Low Adhesive Force. *Macromol. Rapid. Comm.* **2005**, *26* (22), 1805-1809.
10. Khorasani, M. T.; Mirzadeh, H.; Kermani, Z. Wettability of Porous Polydimethylsiloxane Surface: Morphology Study. *Appl. Surf. Sci.* **2005**, *242*, 339-345.
11. Sun, M.; Luo, C.; Xu, L.; Ji, H.; Ouyang, Q.; Yu, D.; Chen, Y. Artificial Lotus Leaf by Nanocasting. *Langmuir.* **2005**, *21* (19), 8978-8981.
12. Ma, M.; Hill, R. M.; Lowery, J. L.; Fridrikh, S. V.; Rutledge, G. C. Electrospun Poly(Styrene-block-dimethylsiloxane) Block Copolymer Fibers Exhibiting Superhydrophobicity. *Langmuir.* **2005**, *21* (12), 5549-5554.

13. Zhao, N.; Xie, Q.; Weng, L.; Wang, S.; Zhang, X.; Xu, J. Superhydrophobic Surface from Vapor-Induced Phase Separation of Copolymer Micellar Solution. *Macromolecules*. **2005**, *38* (22), 8996-8999.
14. Lu, X.; Zhang, C.; Han, Y. Low-Density Polyethylene Superhydrophobic Surface by Control of Its Crystallization Behavior. *Macromol. Rapid. Comm.* **2004**, *25* (18), 1606-1610.
15. Jiang, L.; Zhao, Y.; Zhai, J. A Lotus-Leaf-like Superhydrophobic Surface: A Porous Microsphere/Nanofiber Composite Film Prepared by Electrohydrodynamics. *Angew. Chem. Int. Edit.* **2004**, *43* (33), 4338-4341.
16. Lee, W.; Jin, M. K.; Yoo, W. C.; Lee, J. K. Nanostructuring of a Polymeric Substrate with Well-Defined Nanometer-Scale Topography and Tailored Surface Wettability. *Langmuir*. **2004**, *20*, 7665-7669.
17. Mohammadi, R.; Wassink, J.; Amirfazli, A. Effect of Surfactants on Wetting of Super-Hydrophobic Surfaces. *Langmuir*. **2004**, *20* (22), 9657-9662.
18. Yan, H.; Kurogi, K.; Mayama, H.; Tsujii, K. Environmentally Stable Super Water-Repellent Poly(alkylpyrrole) Films. *Angew. Chem. Int. Edit.* **2005**, *44* (22), 3453-3456.
19. Zhang, J.; Lu, X.; Huang, W.; Han, Y. Reversible Superhydrophobicity to Superhydrophilicity Transition by Extending and Unloading an Elastic Polyamide Film. *Macromol. Rapid. Comm.* **2005**, *26* (6), 477-480.
20. Zhao, N.; Xu, J.; Xie, Q.; Weng, L.; Guo, X.; Zhang, X.; Shi, L. Fabrication of Biomimetic Superhydrophobic Coating with a Micro-Nano-Binary Structure. *Macromol. Rapid. Comm.* **2005**, *26* (13), 1075-1080.
21. Feng, X.; Feng, L.; Jin, M.; Zhai, J.; Jiang, L.; Zhu, D. Reversible Superhydrophobicity to Super-hydrophilicity Transition of Aligned ZnO Nanorod Films. *J. Am. Chem. Soc.* **2004**, *126*(1), 62-63.
22. Yang, Y. H.; Li, Z. Y.; Wang, B.; Wang, C. X.; Chen, D. H.; Yang, G. W. Self-assembled ZnO Agave-like Nanowires and Anomalous Superhydrophobicity. *J. Phys.: Condens. Matter*. **2005**, *17* (35), 5441.
23. Feng, X.; Zhai, J.; Jiang, L. The Fabrication and Switchable

- Superhydrophobicity of TiO₂ Nanorod Films. *Angew. Chem. Int. Edit.* **2005**, *44* (32), 5115-5118.
24. Teshima, K.; Sugimura, H.; Inoue, Y.; Takai, O.; Takano, A. Transparent Ultra Water-Repellent Poly (ethylene terephthalate) Substrates Fabricated by Oxygen Plasma Treatment and Subsequent Hydrophobic Coating. *Appl. Surf. Sci.* **2005**, *244*, 619-622.
 25. Song, X.; Zhai, J.; Wang, Y.; Jiang, L. Fabrication of Superhydrophobic Surfaces by Self-Assembly and Their Water-Adhesion Properties. *J. Phys. Chem. B.* **2005**, *109* (9), 4048-4052.
 26. Guo, Z.; Zhou, F.; Hao, J.; Liu, W. Stable Biomimetic Super-Hydrophobic Engineering Materials. *J. Am. Chem. Soc.* **2005**, *127* (45), 15670-15671.
 27. Qian, B.; Shen, Z. Fabrication of Superhydrophobic Surfaces by Dislocation-Selective Chemical Etching on Aluminum, Copper, and Zinc Substrates. *Langmuir.* **2005**, *21* (20), 9007-9009.
 28. Callies, M.; Chen, Y.; Marty, F.; Pepin, A.; Quere, D. Microfabricated Textured Surfaces for Super-hydrophobicity Investigations. *Microelectron. Eng.* **2005**, *78-79*, 100-105.
 29. Fürstner, R.; Barthlott, W.; Neinhuis, C.; Walzel, P. Wetting and Self-Cleaning Properties of Artificial Superhydrophobic Surfaces. *Langmuir.* **2005**, *21* (3), 956-961.
 30. Martines, E.; Seunarine, K.; Morgan, H.; Gadegaard, N.; Wilkinson, C. D. W.; Riehle, M. O. Superhydrophobicity and Superhydrophilicity of Regular Nanopatterns. *Nano. Letters.* **2005**, *5* (10), 2097-2103.
 31. Shirtcliffe, N.; McHale, G.; Newton, M.; Perry, C.; Roach, P. Porous Materials Show Superhydrophobic to Superhydrophilic Switching. *Chem. Commun.* **2005**, *25*, 3135-3137.
 32. Hikita, M.; Tanaka, K.; Nakamura, T.; Kajiyama, T.; Takahara, A. Super-Liquid-Repellent Surfaces Prepared by Colloidal Silica Nanoparticles Covered with Fluoroalkyl Groups. *Langmuir.* **2005**, *21* (16), 7299-7302.
 33. Zhai, L.; Cebeci, F. Ç.; Cohen, R. E.; Rubner, M. F. Stable Superhydrophobic Coatings from Polyelectrolyte Multilayers. *Nano. Letters.* **2004**, *4* (7),

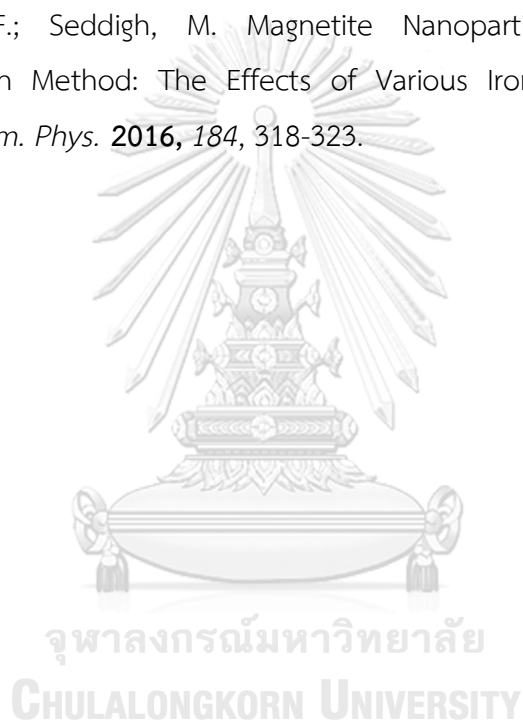
- 1349-1353.
34. Han, J. T.; Jang, Y.; Lee, D. Y.; Park, J. H.; Song, S. H.; Ban, D. Y.; Cho, K. Fabrication of a Bionic Superhydrophobic Metal Surface by Sulfur-induced Morphological Development. *J. Mater. Chem.* **2005**, *15* (30).
 35. Sun, T.; Wang, G.; Liu, H.; Feng, L.; Jiang, L.; Zhu, D. Control over the Wettability of an Aligned Carbon Nanotube Film. *J. Am. Chem. Soc.* **2003**, *125* (49), 14996-14997.
 36. Budy, S. M.; Hamilton, D. J.; Cai, Y.; Knowles, M. K.; Reed, S. M. Polymer Mediated Layer-by-layer Assembly of Different Shaped Gold Nanoparticles. *J. Colloid. Interface. Sci.* **2017**, *487*, 336-347.
 37. Kaboudin, B.; Khanmohammadi, H.; Kazemi, F. Polymer supported gold nanoparticles: Synthesis and characterization of Functionalized Polystyrene-supported Gold Nanoparticles and Their Application in Catalytic Oxidation of Alcohols in Water. *Appl. Surf. Sci.* **2017**, *425*, 400-406.
 38. Li, H.; Men, D.; Sun, Y.; Liu, D.; Li, X.; Li, L.; Li, C.; Cai, W.; Li, Y. Surface Enhanced Raman Scattering Properties of Dynamically Tunable Nanogaps between Au Nanoparticles Self-assembled on Hydrogel Microspheres Controlled by pH. *J. Colloid. Interface. Sci.* **2017**, *505*, 467-475.
 39. Tan, K. H.; Tajuddin, H. A.; Ahmad, R.; Shuhaimi, A.; Johan, M. R. Fabrications of Nanocomposite Gold-Polymer Metamaterials Consisting of Periodic Microcavities with Tunable Optical Properties. *Optik.* **2017**, *150*, 54-61.
 40. Mamdouh, E.; Abdelsalam, P. N. B.; Kelf, T.; Baumberg, J. Wetting of Regularly Structured Gold Surfaces. *Langmuir.* **2005**, *21*, 1753-1757.
 41. Cui, S.; Lu, S.; Xu, W.; An, B.; Wu, B. Fabrication of Robust Gold Superhydrophobic Surface on Iron Substrate with Properties of Corrosion Resistance, Self-cleaning and Mechanical durability. *J. Alloy. Compd.* **2017**, *728*, 271-281.
 42. Ishida, T.; Kuroda, K.; Kinoshita, N.; Minagawa, W.; Haruta, M. Direct Deposition of Gold Nanoparticles onto Polymer Beads and Glucose Oxidation with H₂O₂. *J. Colloid. Interface. Sci.* **2008**, *323* (1), 105-11.
 43. Deore, A. V.; Bhoraskar, V. N.; Dhole, S. D. Low-energy Electron Irradiation

- Assisted Diffusion of Gold Nanoparticles in Polymer Matrix. *Radiat. Phys. Chem.* **2014**, *96*, 97-100.
44. Ahmed, S. R.; Kim, J.; Tran, V. T.; Suzuki, T.; Neethirajan, S.; Lee, J.; Park, E. Y. In situ Self-assembly of Gold Nanoparticles on Hydrophilic and Hydrophobic Substrates for Influenza Virus-sensing Platform. *Sci. Rep.* **2017**, *7*, 44495.
45. Nguyen, N.-T. Micro-magnetofluidics: Interactions between Magnetism and Fluid Flow on the Microscale. *Microfluid. Nanofluid.* **2011**, *12* (1-4), 1-16.
46. Zhao, W.; Cheng, R.; Miller, J. R.; Mao, L. Label-Free Microfluidic Manipulation of Particles and Cells in Magnetic Liquids. *Adv. Funct. Mater.* **2016**, *26* (22), 3916-3932.
47. Zhang, Q.; Xu, J. J.; Liu, Y.; Chen, H. Y. In-situ Synthesis of Poly(dimethylsiloxane)-gold Nanoparticles Composite Films and its Application in Microfluidic Systems. *Lab. Chip.* **2008**, *8* (2), 352-357.
48. Yuan, Y.; Lee, T. R. Surface Science Techniques. **2013**, *51*, 3-34.
49. Young, T. An Essay on the Cohesion of Fluids. **1805**, *95*, 65-87.
50. Brzoska, J. B.; Azouz, I. B.; Rondelez, F. Silanization of Solid Substrates: A Step Toward Reproducibility. *Langmuir.* **1994**, *10* (11), 4367-4373.
51. Nadkarni, G. D.; Garoff, S. Reproducibility of Contact Line Motion on Surfaces Exhibiting Contact Angle Hysteresis. *Langmuir.* **1994**, *10* (5), 1618-1623.
52. Li, X. M.; Reinhoudt, D.; Crego-Calama, M. What Do We Need for a Superhydrophobic Surface? A Review on the Recent Progress in the Preparation of Superhydrophobic Surfaces. *Chem. Soc. Rev.* **2007**, *36* (8), 1350-1368.
53. Wenzel, R. N. Resistance of Solid Surfaces to Wetting by Water. *Ind. Eng. Chem.* **1936**, *28*, 988-994.
54. Cassie, A. B. D.; Baxter, S. Wettability of Porous Surfaces. *T. Faraday. Soc.* **1944**, *40*.
55. Carmichael, N. Linear Polydimethylsiloxanes. **2011**, *55*.
56. Lee, J. N.; Park, C.; Whitesides, G. M. Solvent Compatibility of Poly(dimethylsiloxane)-Based Microfluidic Devices. *Anal. Chem.* **2003**, *75*(23), 6544-6554.

57. McDonald, J. C.; Duffy, D. C.; Anderson, J. R.; Chiu, D. T.; Wu, H.; Schueller, O. J. A.; Whitesides, G. M. Fabrication of Microfluidic Systems in Poly(dimethylsiloxane). *Electrophoresis*. **2000**, *21*(1), 27-40.
58. Insin, N.; Tracy, J. B.; Lee, H.; Zimmer, J. P.; Westervelt, R. M.; Bawendi, M. G. Incorporation of Iron Oxide Nanoparticles and Quantum Dots into Silica Microspheres. *ACS. Nano*. **2008**, *2*, 197-202.
59. Wang, H.; Cui, X.; Guan, W.; Zheng, X.; Zhao, H.; Wang, Z.; Wang, Q.; Xue, T.; Liu, C.; Singh, D. J.; Zheng, W. Kinetic Effects in the Photomediated Synthesis of Silver Nanodecahedra and Nanoprisms: Combined Effect of Wavelength and Temperature. *Nanoscale*. **2014**, *6*(13), 7295-302.
60. Gong, D.; Long, J.; Jiang, D.; Fan, P.; Zhang, H.; Li, L.; Zhong, M. Robust and Stable Transparent Superhydrophobic Polydimethylsiloxane Films by Duplicating via a Femtosecond Laser-Ablated Template. *ACS. Appl. Mater. Interfaces*. **2016**, *8*(27), 17511-17518.
61. Stanton, M. M.; Ducker, R. E.; MacDonald, J. C.; Lambert, C. R.; McGimpsey, W. G. Super-hydrophobic, Highly Adhesive, Polydimethylsiloxane (PDMS) Surfaces. *J. Colloid. Interface. Sci*. **2012**, *367*(1), 502-508.
62. Yong, J.; Yang, Q.; Chen, F.; Zhang, D.; Du, G.; Bian, H.; Si, J.; Yun, F.; Hou, X. Superhydrophobic PDMS Surfaces with Three-dimensional (3D) Pattern-dependent Controllable Adhesion. *Appl. Surf. Sci*. **2014**, *288*, 579-583.
63. Du, X.; Li, J. S.; Li, L. X.; Levkin, P. A. Porous poly(2-octyl cyanoacrylate): a Facile One-Step Preparation of Superhydrophobic Coatings on Different Substrates. *J. Mater. Chem. A*. **2013**, *1*(4), 1026-1029.
64. Ghazanfari, H. R. E.; Ghazanfari, M. H. Application of a Water Based Nanofluid for Wettability Alteration of Sandstone Reservoir Rocks to Preferentially Gas Wetting Condition. *J. Mol. Liq*. **2017**, *232*, 351-360.
65. Nayak, B. K.; Caffrey, P. O.; Speck, C. R.; Gupta, M. C. Superhydrophobic Surfaces by Replication of Micro/nano-structures Fabricated by Ultrafast-laser-microtexturing. *Appl. Surf. Sci*. **2013**, *266*, 27-32.
66. Ramiasa-MacGregor, M.; Mierczynska, A.; Sedev, R.; Vasilev, K. Tuning and

- Predicting the Wetting of Nanoengineered Material Surface. *Nanoscale*. **2016**, 8(8), 4635-4642.
67. Paclawski, K.; Sak, T. Kinetics and Mechanism of the Reduction of Tetrachloroaurate(III) by Formate in Acidic Aqueous Solution. *J. inorg. nucl. Chem.* **1976**, 38, 1545-1547.
68. Polte, J. Fundamental Growth Principles of Colloidal Metal Nanoparticles—a New Perspective. *Cryst. Eng. Comm.* **2015**, 17(36), 6809-6830.
69. Lim, M.-C.; Park, K.; Kim, S.-H.; Ok, G.; Choi, S.-W.; Woo, M.-A. Facile Preparation of Gold-coated Polydimethylsiloxane Particles by In situ Reduction without Pre-synthesized seed. *Colloid. Surface. A*. **2017**, 529, 916-921.
70. Park, K.; Woo, M.-A.; Lim, J.-A.; Kim, Y.-R.; Choi, S.-W.; Lim, M.-C. In situ Synthesis of Directional Gold Nanoparticle Arrays Along Ridge Cracks of PDMS Wrinkles. *Colloid. Surface. A*. **2018**, 558, 186-191.
71. Khalil, M. M. H.; Ismail, E. H.; El-Magdoub, F. Biosynthesis of Au Nanoparticles Using Olive Leaf Extract. *Arab. J. Chem.* **2012**, 5(4), 431-437.
72. Patra, J. K.; Baek, K. H. Novel Green Synthesis of Gold Nanoparticles Using Citrullus Lanatus Rind and Investigation of Proteasome Inhibitory Activity, Antibacterial, and Antioxidant Potential. *Int. J. Nanomedicine*. **2015**, 10, 7253-7264.
73. Bartosewicz, B.; Bujno, K.; Liszewska, M.; Budner, B.; Bazarnik, P.; Plocinski, T.; Jankiewicz, B. J. Effect of Citrate Substitution by Various α -hydroxycarboxylate Anions on Properties of Gold Nanoparticles Synthesized by Turkevich method. *Colloid. Surface. A*. **2018**, 549, 25-33.
74. Simeonova, S.; Georgiev, P.; Exner, K. S.; Mihaylov, L.; Nihtianova, D.; Koynov, K.; Balashev, K. Kinetic Study of Gold Nanoparticles Synthesized in the Presence of Chitosan and Citric Acid. *Colloid. Surface. A*. **2018**, 557, 106-115.
75. Hong, D.; Bae, K.; Hong, S. P.; Park, J. H.; Choi, I. S.; Cho, W. K. Mussel-inspired,

- Perfluorinated Polydopamine for Self-cleaning Coating on Various Substrates. *Chem. Commun.* **2014**, 50(79), 11649-52.
76. Wu, J.; Lee, N. Y. One-step Surface Modification for Irreversible Bonding of Various Plastics with a Poly(dimethylsiloxane) Elastomer at Room Temperature. *Lab. Chip.* **2014**, 14(9), 1564-71.
77. Jopp, J.; Grull, H.; Yerushalmi-Rozen, R. Wetting Behavior of Water Droplets on Hydrophobic Microtextures of Comparable Size. *Langmuir.* **2004**, 20, 10015-10019.
78. Yazdani, F.; Seddigh, M. Magnetite Nanoparticles Synthesized by Co-precipitation Method: The Effects of Various Iron Anions on Specifications. *Mater. Chem. Phys.* **2016**, 184, 318-323.



VITA

NAME Siriwan Boonmeewiriya

DATE OF BIRTH 11 Nov 1993

PLACE OF BIRTH Trang

INSTITUTIONS ATTENDED Chulalongkorn University

HOME ADDRESS 89/129 17 lane Pruklada village Bangtoei Sampran
NakhornPathum 73210

PUBLICATION Proceeding of “ Fabrication of Superhydrophobic Gold
Microstructure on Polymer Substrates ” pp. 44-48.
Pure and Applied Chemistry International Conference
2018
(February 7-9, 2018)

AWARD RECEIVED 1 st Runner-up of Research proposal
Bangkok, Thailand
Thailand Research Expo 2018
(August 9-13, 2018)